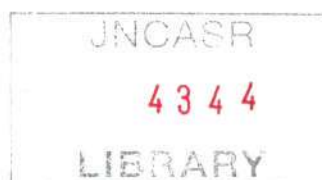



4344



JNCASR LIBRARY  
4344  
  
620.11 P06

**Urea route to the synthesis of metal  
nitrides and to coat one-dimensional  
nanostructures by boron nitride**

A Thesis

submitted in partial fulfillment of the  
requirements of the degree of  
Master of Science [Engg.]

by

A. Gomathi



Chemistry and Physics of Materials Unit  
Jawaharlal Nehru Centre for Advanced Scientific  
Research  
(A Deemed University)  
Bangalore – 560 064  
December 2006

620.11

PO6

## **DECLARATION**

I hereby declare that the matter embodied in this thesis entitled “Urea route to the synthesis of metal nitrides and to coat one-dimensional nanostructures by boron nitride” is the result of investigations carried out by me under the supervision of Prof. C. N. R. Rao, FRS at the Chemistry and Physics of Materials Unit, Jawaharlal Nehru Centre for Advanced Scientific Research, Bangalore, India and that it has not been submitted elsewhere for the award of any degree or diploma.

In keeping with the general practice in reporting scientific observations, due acknowledgement has been made whenever the work described is based on the findings of other investigators.



---

A. Gomathi

## **CERTIFICATE**

I hereby certify that the matter embodied in this thesis entitled “Urea route to the synthesis of metal nitrides and to coat one-dimensional nanostructures by boron nitride” has been carried out by Ms. A. Gomathi at the Chemistry and Physics of Materials Unit, Jawaharlal Nehru Centre for Advanced Scientific Research, Bangalore, India under my supervision and that it has not been submitted elsewhere for the award of any degree or diploma.



---

Prof. C. N. R. Rao, FRS

(Research Supervisor)

## **Acknowledgements**

I am extremely grateful to Prof. C. N. R. Rao, FRS for suggesting me research problems and guiding me throughout. He has been a constant source of inspiration for me. I greatly admire his enthusiasm towards science. I express my hearty gratitude to him for giving me an opportunity to work under his guidance.

I would like to express my sincere thanks to Dr. Govindaraj who has helped me a great deal in carrying out the various experiments. It has been a good learning experience working with him in the lab.

Sincere thanks to Kripasindhu Sardar and Vivekchand for helping me out in the various research problems.

I am thankful to Basavaraj, Usha Madam, Anil, Vasu and Selvi for their help with the various characterization techniques. I thank Neena, Bhuvana and Angappane for their help with the XPS measurements.

I thank Vengadesh, Pranab and Madhu for their help with the magnetic measurements.

I would like to thank my lab members Kanishka, Sandeep and Bhat for their help and co-operation.

I am thankful to the faculty members of JNC. In particular, I would like to thank Prof. G. U. Kulkarni, Prof. Swapan Pati, Prof. Umesh V Waghmare, Prof. Chandrabhas Narayana, Prof. K. S. Narayan, Dr. M. Eswaramoorthy, and Dr. A. Sundaresan for their courses.

My thanks are due to Vengadesh, Bhuvana, Venkat anna and Dinesh for helping me with the thesis.

I am thankful to Shithal, Satish and Vikas of computer lab for their help.

I would like to thank Mrs. Rao for her encouraging words and hospitality.

Special thanks to my friends Deepak, Vivek, Lakshmi, Neena, Kalyani, Reji, Vinod, Sameen, Harish, Vengadesh, Bhuvana, Dinesh, Saiki, Kumar, Claudy, Kanishka, Sandeep, Pearl, Nivas, Minaxie, Thiru, Bheraji, Tamil Selvi, and Devaraj.

Heartfelt thanks to my parents, Shuba, Venkat anna and Dhava for being there for me always.

## **Preface**

Nitrides are the materials of great interest due to their potential applications in various fields of science and technology. A great deal of research is being carried out on their synthesis and properties in order to understand them better. Chapter 1 gives a brief overview of the nitrides.

Chapter 2 deals with the synthesis of the binary nitrides BN, TiN and NbN by urea route and their characterization. Importantly, the products show interesting nanostructural features, as revealed by electron microscopic studies.

In chapter 3 synthesis of ternary nitrides by urea route has been discussed. The ternary nitrides so obtained has been characterized by various physical methods.

Chapter 4 deals the synthesis of super conducting molybdenum nitrides by urea route. It is noteworthy that the nitrides in nanoparticulate regime exhibit superconductivity along with room temperature ferromagnetism, a surface property characteristic of nanoparticles.

Chapter 5 deals with the coating of BN on one-dimensional nanostructures by employing a reaction between urea and boric acid. The BN coating has been characterized by electron microscopic techniques.

## **Contents**

Acknowledgements III

Preface v

<b>1 A brief overview of nitrides.</b> . . . . .	1
1.1 Introduction . . . . .	1
1.2 Ternary nitrides . . . . .	5
1.3 Synthetic strategies for nitrides . . . . .	6
1.4 Nanostructures . . . . .	7
1.5 Synthetic strategies for nanocrystals . . . . .	8
1.6 Synthetic strategies for nanowires. . . . .	10
References . . . . .	12
<b>2 Synthesis of nanostructures of BN, TiN and NbN.</b> . . . . .	15
2.1 Introduction . . . . .	16
2.2 Scope of the present study . . . . .	16
2.3 Experimental and related aspects . . . . .	19
2.4 Results and discussion . . . . .	22
(a) BN nanoparticles . . . . .	22
(b) TiN nanoparticles . . . . .	28
(c) NbN nanoparticles. . . . .	32
2.5 Conclusions . . . . .	36
References . . . . .	37
<b>3 Ternary nitrides: Synthesis and characterization</b>	
3.1 Introduction . . . . .	40



3.2 Scope of the present study. . . . .	40
3.3 Experimental and related aspects. . . . .	42
3.4 Results and discussion . . . . .	44
(a) Characterization of the $\text{Fe}_3\text{Mo}_3\text{N}$ . . . . .	44
(b) Characterization of the $\text{Co}_3\text{Mo}_3\text{N}$ . . . . .	47
(c) Characterization of the $\text{Ni}_2\text{Mo}_3\text{N}$ . . . . .	48
3.5 Conclusions . . . . .	50
References . . . . .	51
<b>4 Superconducting molybdenum nitrides: Synthesis and</b>	
<b>characterization.</b> . . . .	54
4.1 Introduction . . . . .	55
4.2 Scope of the present study. . . . .	56
4.3 Experimental and related aspects. . . . .	57
4.4 Results and discussion . . . . .	58
(a) $\gamma\text{-Mo}_2\text{N}$ nanoparticles. . . . .	58
(b) $\delta\text{-MoN}$ nanoparticles. . . . .	63
4.5 Ferromagnetism in nanoparticles. . . . .	67
4.6 Conclusions . . . . .	71
References . . . . .	72
<b>5 BN coating on one-dimensional nanostructures.</b> . . . .	74
5.1 Introduction . . . . .	75
5.2 Scope of the present study. . . . .	75
5.3 Experimental and related aspects. . . . .	77

5.4 Results and discussion . . . . .	79
5.5 Conclusions . . . . .	89
References . . . . .	90

---

# CHAPTER 1

## A brief overview of nitrides

---

### 1.1 Introduction

Binary nitrides have considerable utility, yet the search for new nitrides has, until recently, been almost completely neglected. R Juza and Y Laurent in Europe and DL Ward in the USA were among the few who published studies of ternary nitrides in the 60s, 70s and early 80s. In the past half dozen years or so, the systematic study of ternary and more complex nitrides has really accelerated. These studies, initiated principally in the groups of R. Kniep and H. Jacobs in Germany and F. J. DiSalvo in the USA, and now continued by these and many other groups, show that the syntheses and structural features of nitrides are often quite different from those of oxides, sulphides or phosphides. Indeed, unique features are often encountered in nitrides.

Nitrogen, the main component of the atmosphere, is omnipresent. The lightest element in the fifth main group plays an important role in chemical compounds, in particular in the nitrides in which the oxidation state of nitrogen is  $-III$ . As shown in Figure 1.1, non-molecular binary

nitrides are not as extensive as binary compounds of oxygen, sulphur or phosphorous, all of which combine with a wider variety of metals, such as the alkali metals, most of the late transition metals, and heavy main-group metals [1-4].

Li Li <sub>3</sub> N	Be Be <sub>3</sub> N <sub>2</sub>											B BN	
	Mg Mg <sub>3</sub> N <sub>2</sub>											Al AlN	Si Si <sub>3</sub> N <sub>4</sub>
Ca Ca <sub>3</sub> N <sub>2</sub>	Sc ScN	Ti TiN Ti <sub>2</sub> N	V VN	Cr CrN Cr <sub>2</sub> N	Mn Mn <sub>3</sub> N <sub>2</sub> Mn <sub>2</sub> N	Fe Fe <sub>3</sub> N Fe <sub>2</sub> N	Co CoN Co <sub>2</sub> N	Ni Ni <sub>3</sub> N Ni <sub>2</sub> N	Cu Cu <sub>3</sub> N	Zn Zn <sub>2</sub> N <sub>2</sub>	Ga GaN	Ge Ge <sub>3</sub> N <sub>4</sub>	
Sr SrN Sr <sub>2</sub> N	Y YN	Zr Zr <sub>3</sub> N <sub>4</sub> ZrN	Nb NbN	Mo MoN Mo <sub>2</sub> N					Ag Ag <sub>3</sub> N	Cd Cd <sub>2</sub> N <sub>2</sub>	In InN		
Ba Ba <sub>3</sub> N <sub>2</sub> Ba <sub>2</sub> N	La LaN	Hf Hf <sub>3</sub> N <sub>4</sub> Hf <sub>2</sub> N <sub>3</sub>	Ta Ta <sub>3</sub> N <sub>5</sub> Ta <sub>2</sub> N	W WN W <sub>2</sub> N	Re Re <sub>2</sub> N					Hg Hg <sub>3</sub> N <sub>2</sub>			Bi BiN
Ce CeN	Pr PrN	Nd NdN		Sm SmN	Eu EuN	Gd GdN	Tb TbN	Dy DyN	Ho HoN	Er ErN	Tm TmN	Yb YbN	Lu LuN
Th Th <sub>3</sub> N <sub>4</sub>		U UN <sub>2</sub>											

**Figure 1.1: The periodic table showing the occurrence of the common binary nitrides.**

In spite of this relatively small number, the nitrides include some extremely useful compounds, for example boron nitride (BN) is used as a high-temperature crucible material, as a lubricant and in abrasives sector. This is because BN does not interact with molten metals and have higher oxidation resistance than carbon [5,6]. Such excellent properties promote the broad applications of BN, which include high-temperature insulators, self-lubricating and heat dissipating coatings, passivation layers, diffusion masks and wear-resistant coatings [7-8].

Among the theoretically possible binary nitrides, many are either nonexistent or have until now not been applied in a pure and well-defined form because of their low stability.  $\text{Li}_3\text{N}$  exhibits an unusually high tendency for formation, the reaction between lithium metal and molecular nitrogen starts at room temperature and atmospheric pressure. In contrast, there is no reliable evidence for the existence and the stability of analogous compounds of the heavier alkali metals. Apparently in the nitrides  $\text{M}_3\text{N}$  ( $\text{M} = \text{Na}, \text{K}, \text{Rb}, \text{Cs}$ ) the high formal charge of the nitride ion make it impossible to form a stable ionic compound. For the alkaline earth metals, binary nitrides with the composition  $\text{M}_3\text{N}_2$  are known for all elements.

In contrast to the ionic structures of the nitrides of lithium and alkaline earth metals, the elements from the third group onwards form nitrides with more covalent character. As the group number increases,

the heavier homologues in their highest oxidation state show a clearly decreasing tendency towards the stable binary nitride formation.

In the synthesis of nitrides, the dominant factor in nitride thermodynamics is the strong N<sub>2</sub> triple bond (941 kJ mol<sup>-1</sup> versus 500 kJmol<sup>-1</sup> for O<sub>2</sub>, for example). The enthalpy of dissociation of N<sub>2</sub>, which is about two times larger than that of the O<sub>2</sub> molecule makes direct reaction with nitrogen sometimes difficult. This also implies that nitriding reactions are generally high-temperature reactions and that they often involve nitrogen containing species, such as ammonia, which are more reactive than molecular nitrogen [9].

Compared with the corresponding oxides, the thermal dissociation of many nitrides with evolution of N<sub>2</sub> occurs at much lower temperatures. Thus, the elimination of N<sub>2</sub> from Si<sub>3</sub>N<sub>4</sub> occurs at atmospheric pressure at about 2173 K, while SiO<sub>2</sub> can be heated above 2273 K [10]. The affinity of most elements for oxygen is larger than that for nitrogen, thus the bond energies for element-oxygen bonds are generally higher than those of the corresponding element-nitrogen bonds. The formation of oxides is thus an important side reaction in the synthesis of nitrides. Thus, the preparation of nitrides in a pure state requires the complete exclusion of oxygen and this has certainly played an important role in hindering a detailed investigation of nitrides.

The above factors often make the solid state chemistry of the nitrides unusual and sometimes unique.

## **1.2 Ternary nitrides**

Ternary nitrides have largely been the focus of recent synthetic research in nitrides, and recent partial reviews of synthetic methods are available [4,9]. The vast majority of recently reported ternary nitrides contain an electropositive element along with a transition metal or later main-group metal. The electropositive element is included to increase the stability of a given nitride, via the inductive effect [11]. A particularly clear example of the stabilizing influence of the electropositive element is the difference between  $\text{Ni}_3\text{N}$  and  $\text{CaNiN}$ , both formally containing  $\text{Ni}^+$ .  $\text{Ni}_3\text{N}$  decomposes to  $\text{N}_2$  and  $\text{Ni}$  even under one atmosphere of  $\text{N}_2$  pressure by 973 K. In contrast,  $\text{CaNiN}$  [12] is made from  $\text{Ca}_3\text{N}_2$  and  $\text{Ni}$  metal at 1273 K, and remains stable under  $\text{N}_2$  to about 1373 K. Studies of ternary nitride materials have become important because of their potential technological applications [3]. Interstitial ternary nitride materials are interesting as they combine the physical properties of ceramics and electronic properties of metals [13]. Unfortunately, ternary nitride class of compounds is not explored much because of their synthetic challenges.

### **1.3 Synthetic strategies for nitrides**

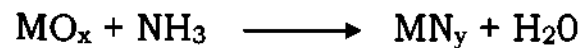
In this session only two basic methods for the preparation of the nitrides are described. They both resort to a gas + solid reaction.

The first method consists of synthesizing a nitride through the direct combination of elements. This method is commonly used with electropositive metals such as rare earth metals. The nitriding temperature is generally between 1073 K and 1473 K and depends on the mutual reactivity of both elements. The difficulty in preparing these nitrides lies mainly in the precautions which need to be taken, since traces of both moisture and oxygen must be avoided. At a given temperature, the reactivity of an element for oxygen is always greater than that for nitrogen. Thus, under nitriding conditions, a very low oxygen partial pressure is enough to irreversibly cause the displacement of nitrogen and the formation of an oxygenated product.

The second method concerns the reaction of ammonia with an oxide. This process can be used to prepare both nitrides and oxynitrides. Ammonia acts both as a reducing and as a nitriding agent. The reaction is carried out in flowing gas, and not under a static atmosphere as in the first method. The rate of ammonia flow depends on the temperature of the reaction: the higher the temperature, the higher the rate, because the dissociation of  $\text{NH}_3$  into nitrogen and hydrogen must be minimized before there is any contact with the product. It has been shown that an



equivalent mixture of nitrogen + hydrogen has no effect on oxides under the same conditions. The general equation is:



It is clear that the reaction is not total: part of the ammonia is dissociated, and nitrogen and hydrogen coming from this dissociation help drive away the water produced by the reaction. This method, which uses, from a thermodynamic point of view, an out-of equilibrium reaction, is especially well-suited for the nitriding of refractory oxides.

#### **1.4 Nanostructures**

As atoms are brought together in a periodic arrangement to form a crystalline solid they lose their identity. This in turn provides structural anisotropy in crystalline materials that reflects in properties like magnetic moment and electrical conductivity. Thus there exists a cross-over region where the individual atomic wave functions tend to lose their identity in order to achieve the wave function of bulk solids. This cross-over region is generally in the 'nano' regime. The word 'nano' refers to  $10^{-9}$ . The objects which have dimensions in the range of hundreds of nanometers are named as nanomaterials.

Nanomaterials are differentiated by their dimensionality. Nanocrystals are zero-dimensional (0D), nanowires and nanotubes are one-dimensional (1D) and thin films are two-dimensional (2D) materials.

### **1.5 Synthetic strategies for nanocrystals**

Nanocrystals, nanowires and nanotubes of a large number of inorganic materials have been synthesized and characterized in the last few years [14-16]. There are two different synthetic approaches to the synthesis of nanomaterials. The first one is the 'top-down' approach, where a bulk material is divided into small pieces to produce nanostructures. Different physical methods such as laser ablation, reactive sputtering, and vacuum evaporation have been employed in this approach. The other procedure is the 'bottom-up' approach. In this, the nanostructures are prepared by controlled assembly of constituent atoms. This method mainly involves chemical routes where different precursors are reacted in presence of suitable stabilizing agents for controlled growth of nanostructures. In the following section we discuss some of the important synthetic strategies for the preparation of the nanostructures.

Preparation of 0D nanocrystals by means of top-down approach has not been a success due to the high energy associated with the process and the particles always tend to aggregate to give bigger crystals.

Because of its inherent simplicity, the bottom-up approach is attractive. The first report on nanoparticles was the controlled precipitation of dilute colloidal solutions [16-19]. In a typical synthesis, bare ions or atoms are reacted with each other at high temperature in a solution. This is done by rapid injection of one reagent into a hot solution containing other reagent in a required molar ratio. The growth process is known as Ostwald ripening. Successful controlled synthesis of colloidal particles is restricted to metals, metal oxides and metal chalcogenides. However there are a few reports on the preparation of some arsenide and phosphide nanocrystals [20].

### **Solvothermal technique:**

It is a soft chemical process for the preparation of nanocrystals. In this technique the reaction is carried out in an autoclave with suitable reactants and solvent which is then heated to the desired temperature. This method can effectively prevent the products from oxidizing and have used to synthesize a number of compounds. Synthesis of TiN and NbN nanocrystals by the benzene-thermal route (using  $\text{TiCl}_4$  in the case of TiN and  $\text{NbCl}_5$  for NbN and  $\text{NaN}_3$ ) is an example for the solvothermal route [21,22].

## **1.6 Synthetic strategies for nanowires**

The 1D nanowire of a material is formed by the crystallization in mainly one direction. The growth of a crystal from a vapor, liquid or solid phase involves two fundamental steps, namely nucleation and growth. As the concentration of the building units becomes sufficiently high, they aggregate and nucleation takes place. These nuclei serve as seed for further growth to form larger clusters. It is not trivial to control this phase transition process. When developing a synthetic method for nanostructures, the most important features that have to be controlled are dimension, shape and uniformity. Anisotropic nature of the crystallographic structure of solids can be promoted for 1D growth [23]. Introduction of a solid-liquid interface can also result in preferential one-dimensional growth [24]. Another simple way of synthesizing 1D nanostructure is to use one-dimensional porous templates [25]. Controlling the super saturation of a seed can modify the growth preferentially in one direction [26]. Usage of capping agents can kinetically control the growth rates of various facets of a crystal [27]. Self-assembly of 0D nanocrystals can also lead to 1D nanostructures [28]. And finally reducing the size of a microstructure by a top-down approach can result in 1D nanostructure formation [29]. Thus some of the well established routes for the synthesis of nanowires are laser-

assisted catalytic growth, chemical vapor deposition, template-assisted synthesis and vapor-liquid-solid (VLS) growth process.

### **Vapor-liquid-solid mechanism:**

The growth of one-dimensional crystalline structures by introduction of a liquid-solid interface in vapor phase was observed and extensively studied by Wagner and Ellis in 60s [30-31]. They proposed that the symmetry of the isotropic crystal breaks if three phases are present in equilibrium in a system. This is VLS process. Following this mechanism a number of one-dimensional nanostructures have been synthesized. In the VLS process, a metal particle is used which forms a liquid alloy (at a temperature higher than the eutectic point) with the material supplied in vapor phase. The liquid alloy gets super-saturated when more growth material is supplied at this temperature. This results in nucleation and growth in one direction at the solid-liquid interface. Validity of this process was demonstrated by Wu et al. who monitored high-temperature growth stages of Ge nanowires in the presence of Au catalyst in-situ in TEM [32]. Metal particles act as catalyst as they are never consumed during growth and can therefore be seen at the tips of the nanowires. This provides a control over the diameter of the structure that is now dictated by the size of the catalyst particle and remains essentially unchanged during the entire growth.

## References

- [1]. L. E. Toth, Transition Metal Carbides and Nitrides, Academic Press, New York, 1971.
- [2]. G. V. Samsonov, I. M. Vinitiskii, Handbook of Refractory Compounds, Academic Press, New York, 1980.
- [3]. S. T. Oyama, The Chemistry of Transition Metal Carbides and Nitrides, Blackie Academic Professional, Glasgow, 1996.
- [4]. N. E. Brese, M. O'Keefe, Structure and Bonding, 79, 1992, 307.
- [5]. L. A. Chernozatonskii, E. G. Galpern, I. V. Stankevich, Y. K. Shimkus, Carbon, 37, 1999, 117.
- [6]. D. Goldberg, Y. Bando, M. Mitome, K. Kurashima, N. Grobert, M. Reyes-Reyes, H. Terrones, M. Terrones, Chem. Phys. Lett., 360, 2002, 1.
- [7]. S. P. S. Arya, A. D. Amico, Thin Solid Films, 157, 1988, 267.
- [8]. P. B. Mirkarimi, K. F. McCarty, D. L. Medlin, Mater. Sci. Eng., 21, 1997, 47.
- [9]. R. Marchand, Y. Laurent, J. Guyader, P. L'Haridon, P. Verdier, J. Eur. Ceram. Soc., 8, 1991, 197.
- [10]. W. Schnick, Angew. Chem. Int. Ed. Engl. 32, 1993, 806.
- [11]. J. Etourneau, J. Portier, F. Menil, J. All. Comp. 188, 1992, 1.
- [12]. M. Y. Chem, F. J. DiSalvo, J. Solid State Chem., 88, 1990, 459.
- [13]. S. T. Oyama, J. Solid State Chem., 96, 1992, 442.
- [14]. S. Iijima, Nature, 354, 1991, 56.

- [15]. Y. Xia, P. Yang, Y. Sun, Y. Wu, B. Mayers, B. Gates, Y. Yin, F. Kim, H. Yna, *Adv. Mater.* 15, 2003, 353.
- [16]. C. N. R. Rao, B. C. Satishkumar, A. Govindaraj, M. Nath, *ChemPhysChem*, 2, 2001, 78.
- [17]. V. K. La Mer, R. H. Dinegar, *J. Am. Chem. Soc.* 72, 1950, 4847.
- [18]. R. Rossetti, S. Nakahnara, E. L. Brus, *J. Chem. Phys.* 79, 1983, 1986.
- [19]. A. Henglein, *Pure. Appl. Chem.* 56, 1984, 1215.
- [20]. J. R. Heath, J. J. Shiang, *Chem. Soc. Rev.* 27, 1998, 65.
- [21]. J. Hu, Q. Lu, K. Tang, S. Yu, Y. Qian, G. Zhou, X. Liu, *J. Am. Ceram. Soc.*, 83, 2000, 430.
- [22]. J. Ma, Y. Du, Y. Qian, *Journal of Alloys and Compounds* 389, 2005, 296.
- [23]. B. Mayers, B. Gates, Y. Yin, Y. Xia, *Adv. Mater.* 13, 2001, 1380.
- [24]. T. J. Trentler, K. M. Hickman, S. C. Goel, A. M. Viano, P. C. Gibbons, W. E. Buhro, *Science*, 270, 1995, 1791.
- [25]. A. Gustafsson, F. Reinhardt, G. Biasiol, E. Kapon, *Appl. Phys. Lett.* 67, 1999, 3673.
- [26]. G. S. Cheng, L. D. Zhang, Y. Zhu, G. T. Fei, L. Li, *Appl. Phys. Lett.* 75, 1999, 2455.
- [27]. N. Wang, Y. H. Tang, Y. F. Zhang, C. S. Lee, I. Bello, S. T. Lee, *Chem. Phys. Lett.* 299, 1999, 237.

- [28]. X. Peng, L. Manna, W. Yang, J. Wickman, E. Scher, A. Kadavanich, A. P. Alivisatos, *nature*, 404, 2000, 59.
- [29]. Z. Tang, N. A. Kotov, M. Giersig, *Science*, 297, 2002, 237.
- [30]. R. S. Wagner. *Whisker Technology* (Ed: Levitt AP), Wiley-Interscience, New York, 1970.
- [31]. R. S. Wagner, W. C. Ellis, *Appl. Phys. Lett.* 84, 1964, 89.
- [32]. Y. Wu, P. Yang, *J. Am. Chem. Soc.* 123, 2001, 3165.



---

## **CHAPTER 2**

### **Synthesis of nanostructures of BN,**

### **TiN and NbN\***

---

#### **Summary**

This chapter of the thesis deals with the synthesis and characterization of the nanostructures of the binary nitrides BN, TiN and NbN. By heating mixtures of  $\text{H}_3\text{BO}_3$ ,  $\text{TiCl}_4$ , and  $\text{NbCl}_5$  with urea in 1:6 molar ratios in the 1173-1273 K range, nanoparticles of BN, TiN and NbN have been obtained respectively. The nanoparticles are crystalline and have been characterized by electron microscopy and other techniques. By carrying out the urea reaction over Au islands deposited on Si substrates, nanowires of TiN could be obtained.

---

\* Paper based on this work has been published in Mater. Res. Bull. (2006)

## **2.1 Introduction**

Hexagonal boron nitride (BN) has a layered, graphite-like structure, consisting of  $B_3N_3$  hexagons. Besides its high-temperature stability, chemical inertness and hardness, BN also exhibits potential applications [1-4] as UV-detectors, cold cathode materials and gate-insulators for metal-insulator-semiconductor field-effect-transistors (MISFETs). Titanium nitride (TiN) which crystallizes in a B1 structure, space group  $Fm\bar{3}m$ , may occur in a wide range of compositions [5-6]. TiN exhibits a very broad range of interesting and potentially valuable physical and chemical properties. TiN has been utilized to provide wear-resistant coatings for cutting tools [7] and diffusion barriers in silicon semiconductor devices [8]. Its optical properties, similar to those of gold, make it of special interest for solar energy applications [9]. Among the transition metal nitrides, niobium nitride (NbN) has received a great deal of attention, owing to its high hardness [10], high wear resistance [11], high melting point [12], good temperature stability, good chemical stability at high temperature [13] and superconducting properties [14].

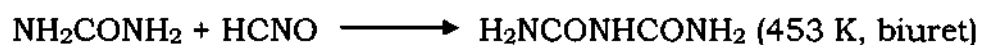
## **2.2 Scope of the present study**

Exploring synthetic methods for binary metal nitrides such as BN, TiN, and NbN is of interest because of the useful properties of these materials. These nitrides have been prepared by various means in bulk form and in some instances in the form of nanostructures. Chopra et al.

[15] reported the synthesis of BN nanotubes by arc discharge between a BN-packed tungsten rod and a cooled copper electrode. Synthesis of BN nanotubes starting from boron powder, iron oxide and ammonium chloride has been reported [16]. Deepak et al. [17] have reported MWNT/activated carbon assisted synthesis of BN nanotubes and nanowires from boric acid. The synthesis of single-crystalline TiN nanorods by the metathesis reaction between  $\text{TiCl}_4$  and  $\text{NaN}_3$  was reported recently by Joshi et al. [18], while the preparation of TiN nanocrystals by the reaction of  $\text{TiCl}_4$  and  $\text{NaNH}_2$  was reported by two groups [19,20]. The metathesis reaction involving  $\text{TiCl}_3$  and  $\text{Ca}_3\text{N}_2$  also produces TiN nanorods [21]. Niobium nitride (NbN) nanocrystals were prepared by the reaction of  $\text{NbCl}_5$  with  $\text{NaN}_3$  by Shi et al. [22]. The benzene-thermal route has also been employed to synthesize NbN [23].

We have sought to develop a simple synthetic method for BN, TiN, and NbN, with specific interest in their nanostructures. For this purpose, we have chosen the urea route which involves heating a mixture of urea with an appropriate compound of boron, titanium and niobium at an appropriate temperature. In the past few years, there has been some effort to prepare metal nitrides using urea ( $\text{NH}_2\text{CONH}_2$ ), which is readily available and is environmentally benign. The idea behind using urea is motivated by the fact that heating urea at 423 K is known to yield  $\text{NH}_3$  and thereby can replace hazardous precursors used as traditional

nitrogen sources. Pure urea decomposes endothermically in several stages [24].



In oxygen free atmosphere non-oxygen containing products,  $\text{H}_2\text{CN}_2$ ,  $\text{H}_4\text{C}_2\text{N}_4$  and  $\text{H}_6\text{C}_3\text{N}_6$  are also formed. On heating to higher temperatures however, all the nitrogen compounds decompose. In 1995 Podsiadlo et al. [24,25] demonstrated that when urea reacts with Ga or In metal in a  $\text{N}_2$  atmosphere it forms a mixture of metal nitrides and oxides. They could obtain pure GaN only by reacting Ga metal with urea in an ammonia atmosphere at 1123 K. In another experiment they obtained a mixture of InN,  $\text{In}_2\text{O}_3$  and In metal at 973 K by the reaction of In metal with urea. The formation of pure InN took place only when the reaction was performed in an ammonia atmosphere.

We have attempted to investigate whether this simple procedure of urea route could be used to synthesize the binary nitrides of boron, titanium and niobium and we have successfully prepared BN, TiN and NbN. Importantly, the products show interesting nanostructural features, as revealed by electron microscopic studies.

## **2.3 Experimental and related aspects**

### **(a) Synthesis of nitrides**

The basic synthetic procedure employed for the three nitrides was to heat a compound of boron, titanium or niobium with urea at an appropriate temperature. The compounds used for this purpose were  $\text{H}_3\text{BO}_3$ ,  $\text{TiCl}_4$ , and  $\text{NbCl}_5$ .

In the synthesis BN, 100 mg of  $\text{H}_3\text{BO}_3$  and 600 mg of urea, taken in the molar ratio 1:6 was ground to give an intimate mixture. The mixture was then taken in an alumina boat and heated in a tube furnace at 1273 K for 3 h in a  $\text{N}_2$  atmosphere.

In the case of TiN, a  $\text{TiCl}_4$ -urea complex (titanium:urea::1:6) was prepared by mixing  $\text{TiCl}_4$  in acetonitrile with urea. In order to synthesize the  $\text{TiCl}_4$ -urea complex, about 0.2 ml of  $\text{TiCl}_4$  was dissolved in acetonitrile to give a yellow solution and to this was added 700 mg of urea dissolved in acetonitrile. The solution was stirred for 2 h to ensure the completion of the reaction. Then the complex was heated at 1173 K for 3 h in a  $\text{N}_2$  atmosphere. The golden yellow product obtained at the end of the reaction was collected for further analysis.

TiN nanowires were prepared by thermal decomposition of  $\text{TiCl}_4$ -urea complex in the presence of gold nanoclusters as catalyst. First 10-20 nm thick films of Au nanoclusters were deposited using DC sputtering

technique on selected area of Si (100) substrates by the help of a mask. In each reaction approximately 30-50 mg of the  $\text{TiCl}_4$ -urea complex was placed on the top of the Au coated Si (100) substrates on an alumina boat. Figure shows the schematic of the experimental set up.

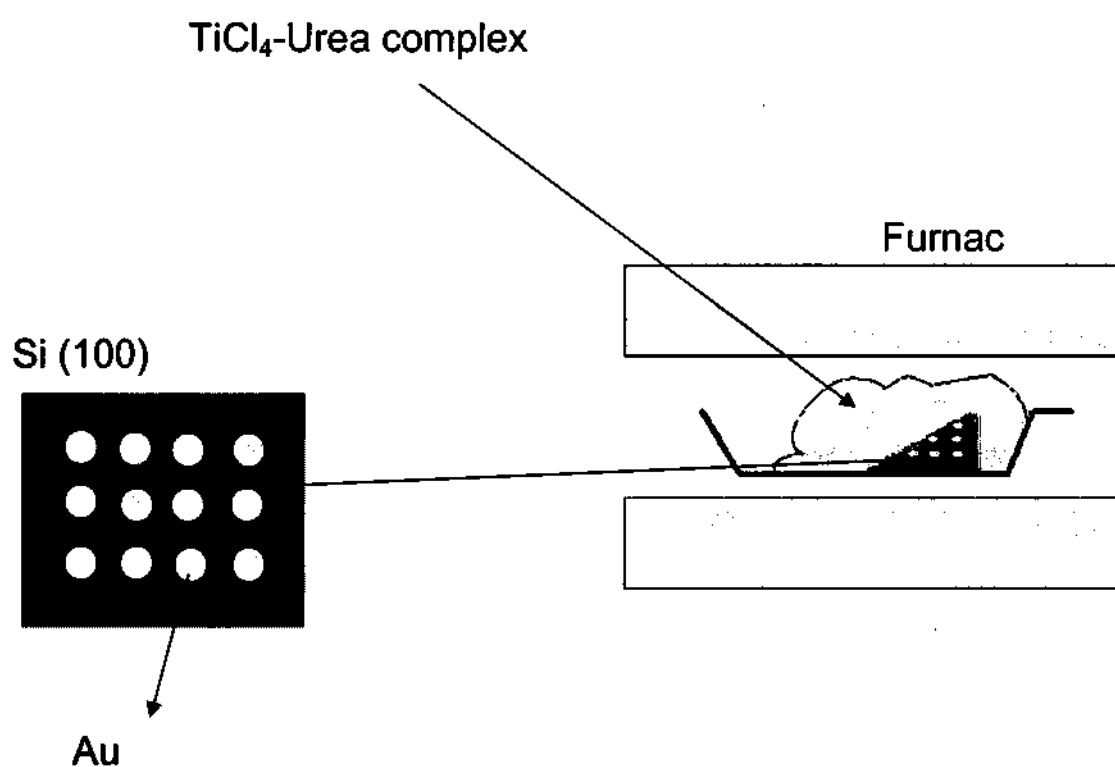


**Figure 2.1: Schematic of the strategy used for the growth of TiN nanowires.**

To synthesize NbN nanoparticles, a mixture of 100 mg NbCl<sub>5</sub> and 150 mg urea taken in the molar ratio 1:6 was ground well and the resulting mixture was heated at 1173 K for 3 h in a N<sub>2</sub> atmosphere. The resulting product was silver-grey in color.

### **(b) Characterization Techniques**

**X-ray Diffraction:** X-ray diffraction (XRD) patterns of the nitrides were recorded using Cu K $\alpha$  radiation on a Rich-Siefert XRD-3000-TT diffractometer.

**Scanning electron microscopy:** Scanning electron microscope (SEM) images were obtained using a LEICA S440i SEM.

**Transmission electron microscopy:** For transmission electron microscopy, the nitrides were dispersed in CCl<sub>4</sub> and dropped on to the holey carbon-coated copper grids. The grids were allowed to dry in the air. Transmission electron microscope (TEM) images were obtained with a JEOL JEM 3010, operating with an accelerating voltage of 300 kV.

**Thermogravimetric analysis:** Thermogravimetric analysis (TGA) was carried out on a Mettler-Toledo-TG-850 instrument.

**X-ray photoelectron spectroscopy:** X-ray photoelectron spectra (XPS) were recorded with an ESCALAB MKIV spectrometer employing AlK $\alpha$  radiation (1486.6 eV).

**Raman spectroscopy:** Raman spectra were recorded with a LabRAM HR with the 633 nm line from HeNe laser. The excitation wavelength is 632.8 nm.

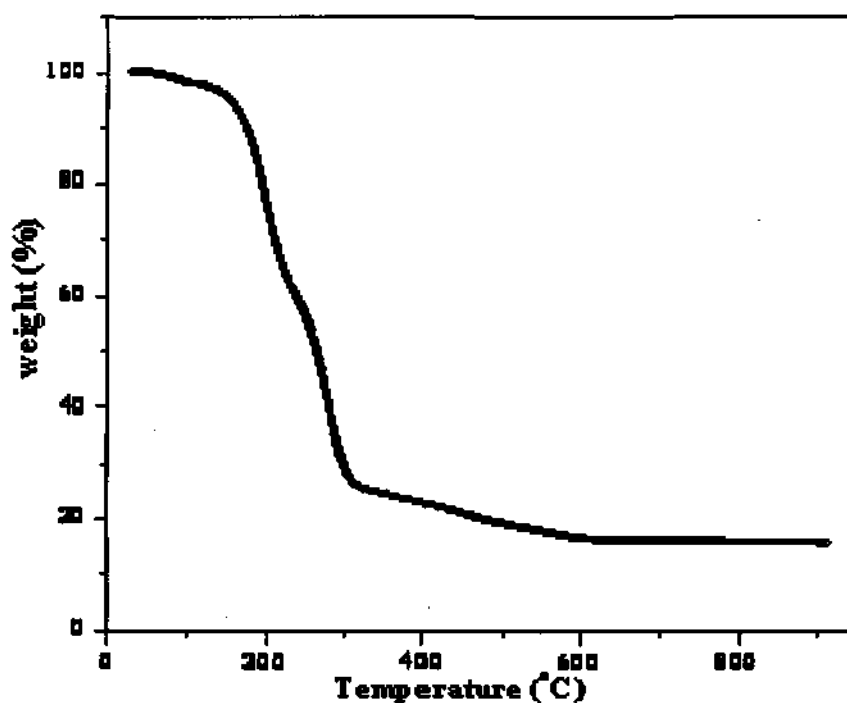
**Magnetic properties:** Magnetic measurements of the as-prepared powder samples were carried out with a vibrating sample magnetometer in Physical Property Measurements System (PPMS, Quantum Design).

## **2.4 Results and Discussions**

### **(a) Characterization of the BN nanoparticles**

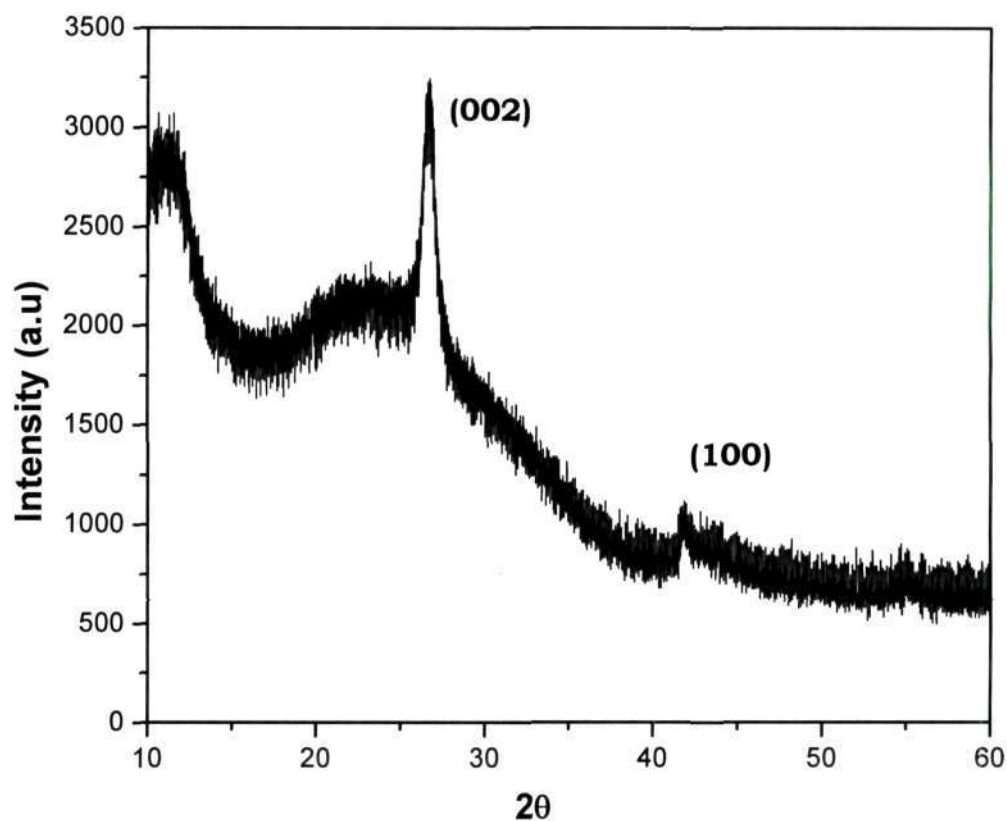
The TGA curve shown in Figure 2.2 is of the mixture of H<sub>3</sub>BO<sub>3</sub> and urea in 1: 12 molar ratio recorded under N<sub>2</sub>. It showed the end product to be BN.





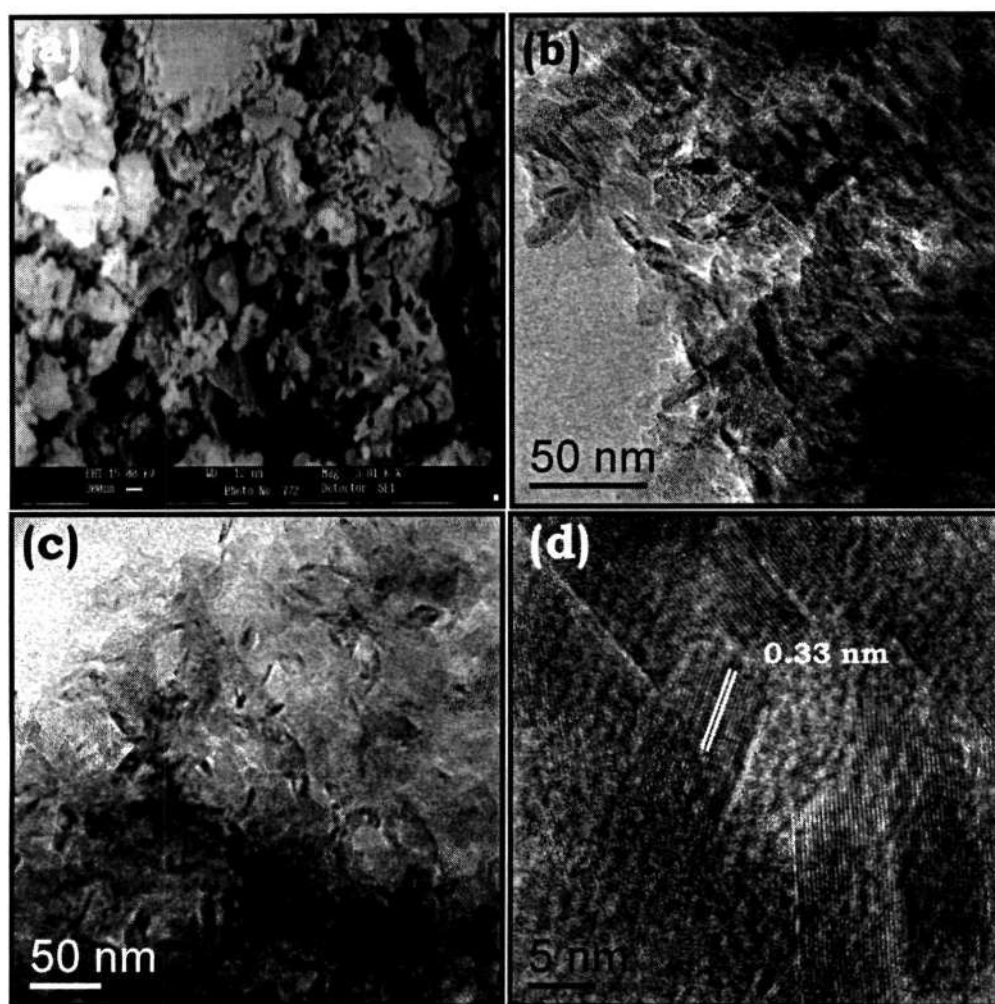
**Figure 2.2: TGA curve of  $H_3BO_3$ :urea::1:12 in a  $N_2$  atmosphere giving BN as the final product.**

The formation of h-BN by heating  $H_3BO_3$  and urea mixture is ascertained by the XRD pattern given in Figure 2.3. The pattern could be indexed with the space group  $P6_3/mmc$  (JCPDS card no: 34-0421). From the pattern it is seen that the lines are rather broad and it may be due to small particle size. By making use of the line widths, the average particle size of the h-BN is calculated from Scherrer formula and it is estimated to be 10 nm. The lattice parameters of the 10 nm particle of h-BN are  $a = 2.57 \text{ \AA}$  and  $c = 6.70 \text{ \AA}$ .



**Figure 2.3: XRD pattern of BN nanoparticles.**

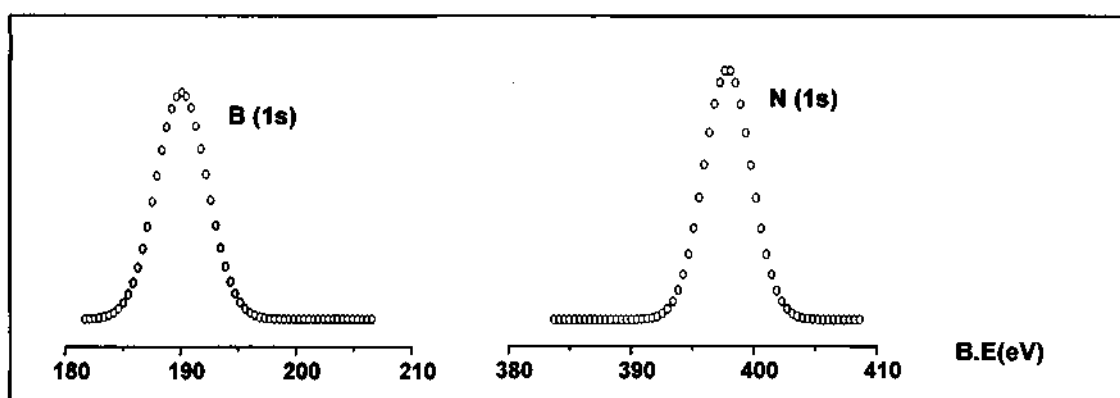
In Figure 2.4 is given the electron microscope images of the BN nanoparticles. Figure 2.4 (a) is the SEM image of the BN nanoparticles. In Figures 2.4 (b) and (c), we have given the TEM images of the BN nanoparticles the particles appear to be rod-like and ~10 nm long in agreement with that estimated from XRD data. Figure 2.4 (d) is the high



**Figure 2.4: (a) SEM image of the BN particles. (b) and (c) TEM images of the BN nanoparticles. (d) HREM image of the BN nanoparticles.**

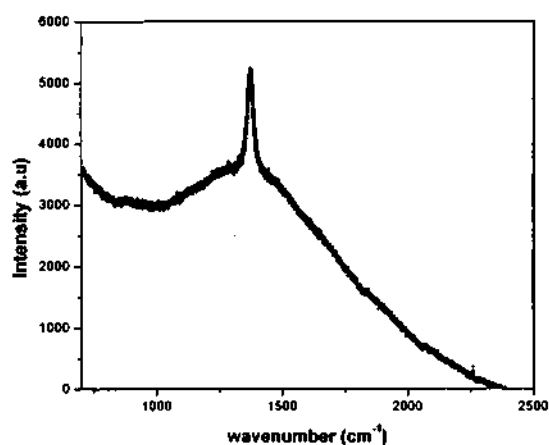
resolution electron microscope (HREM) image of the BN nanoparticles and it shows a lattice spacing of 0.33 nm corresponding to the spacing between the (002) planes of h-BN.

We have characterized the nanoparticles of BN by XP spectrum. Figure 2.5 gives the XP spectrum of the nanoparticles which gives the characteristic binding energy (B.E) of 190 eV for B (1s) and 397.8 eV for N (1s).



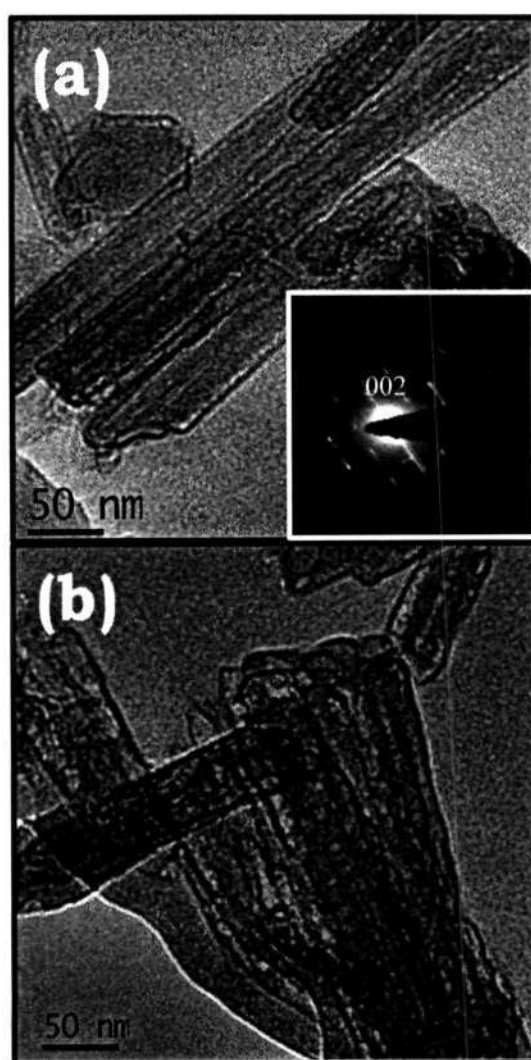
**Figure 2.5: X-ray photoelectron spectrum of BN**

Figure 2.6 gives the Raman spectrum of the BN nanoparticles. The spectrum shows a dominant peak centered at  $1372\text{ cm}^{-1}$ , corresponding to the  $E_{2g}$  vibrational mode of h-BN.



**Figure 2.6: Raman spectrum of BN nanoparticles**

Heating the 1:6  $\text{H}_3\text{BO}_3$ -urea mixture for a longer duration of 12 h at 1273 K produced BN nanotubes. Figure 2.7 (a) and (b) give the TEM images of the BN nanotubes so obtained. The inset in the Figure 2.7 (b) shows the selected area electron diffraction (SAED) pattern of the BN nanotubes with an interlayer spacing 0.33 nm characteristic of the (002) planes.



**Figure 2.7: (a) and (b) TEM images of the BN nanotubes with the inset in (a) showing the SAED pattern of a tube.**

### **(b) Characterization of the TiN nanoparticles**

The golden yellow product of heating a 1:6 mixture of  $\text{TiCl}_4$  and urea gave a XRD pattern shown in Figure 2.8, characteristic of cubic TiN. The pattern could be indexed with the  $Fm\bar{3}m$  space group (38-1420) with the lattice parameter  $a = 4.17 \text{ \AA}$ . From the Scherrer equation based on XRD line-widths the particle size is estimated to be 35 nm.

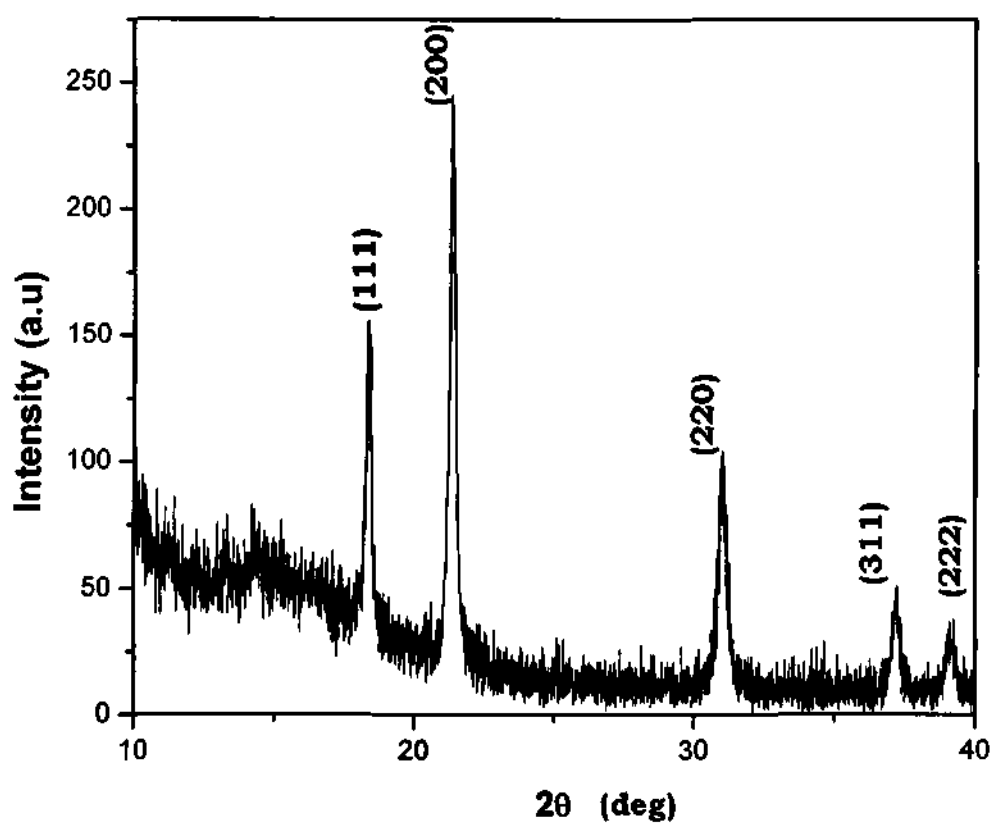
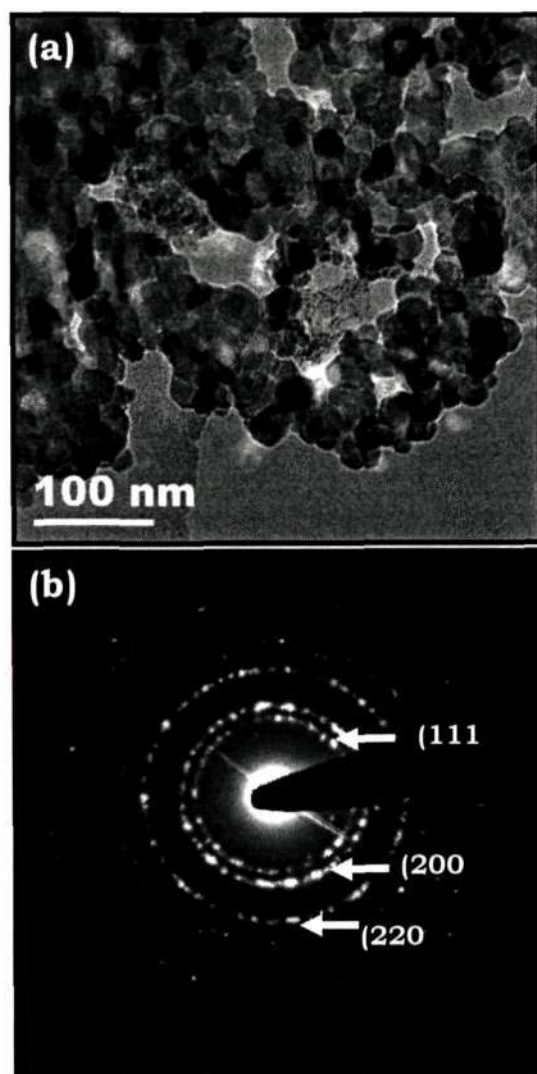


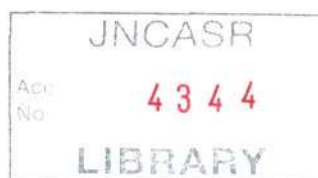
**Figure 2.8: XRD pattern of TiN nanoparticles.**

In Figure 2.9 (a) we show a TEM image of TiN nanoparticles. The average particle size is around 35 nm and is comparable to that estimated from the XRD pattern. The SAED pattern shown in Figure 2.9 (b) shows the rings corresponding to (111), (200) and (220) planes.



620.11  
p06

**Figure 2.9: (a) TEM image of TiN nanoparticles. (b) SAED pattern of the TiN nanoparticles.**



We characterized the TiN nanoparticles by XPS. The XP spectrum given in Figure 2.10 gives characteristic BE values of 455 and 461 eV for Ti ( $2p_{3/2}$ ) and Ti ( $2p_{1/2}$ ) respectively and 397 eV for N (1s).

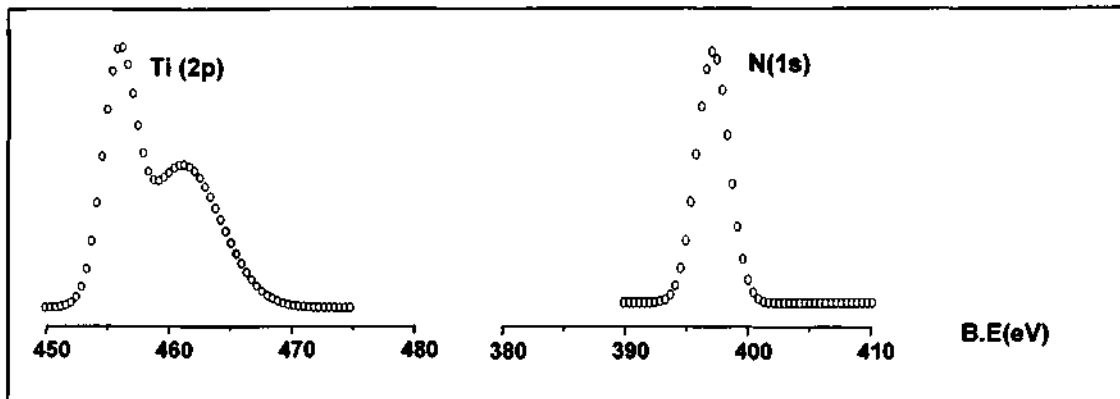


**Figure 2.10: X-ray photoelectron spectrum of TiN**

Figure 2.11 is the Raman spectrum of the TiN nanoparticles which shows four broad bands between 200 and 600  $\text{cm}^{-1}$  in agreement with the literature.

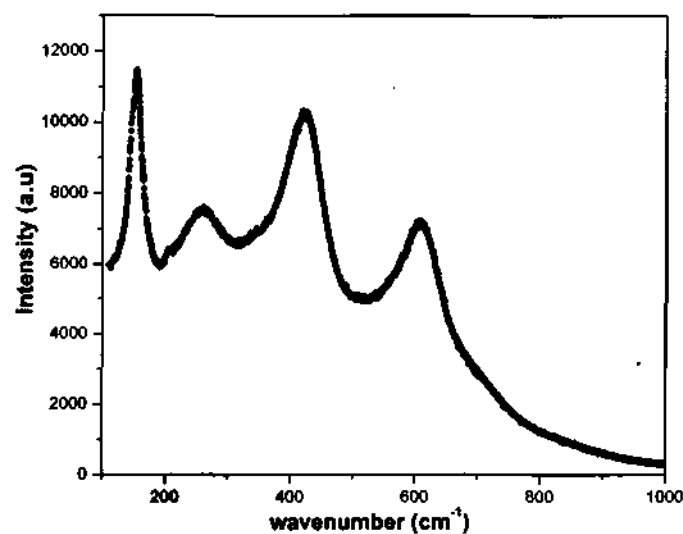


**Figure 2.11: Raman spectrum of TiN nanoparticles.**



In order to prepare TiN nanowires we used Au coated Si substrates. The reaction carries out on these resulted in the formation of TiN nanowires on the Au islands as shown in the SEM image in Figure 2.12 (a). In Figure 2.12 (b) and (c) are shown the TEM images of the TiN nanowires. In Figure 2.12 (d) we show the SAED pattern of a TiN nanowire. It clearly shows the pattern corresponding to the (111) and (200) planes.

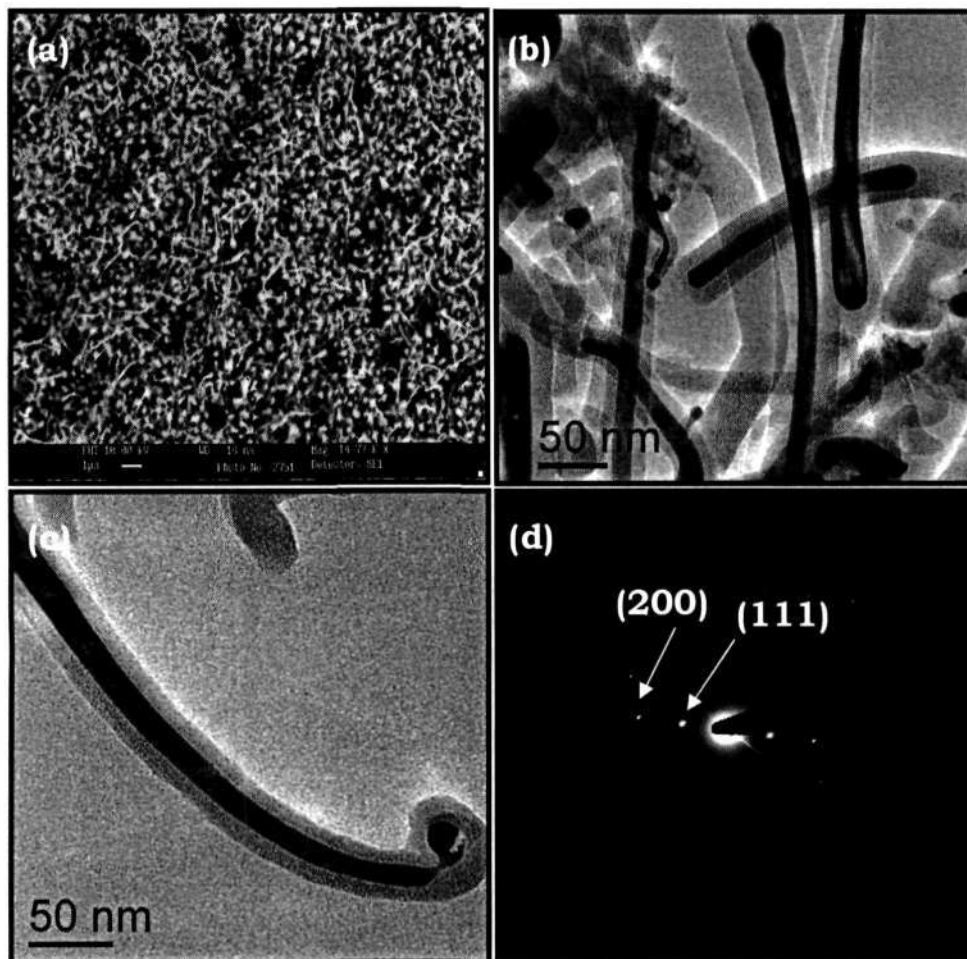


**Figure 2.12: (a) SEM image of the TiN nanowires. (b) and (c) TEM images of the TiN nanowires. (d) SAED pattern of a TiN nanowire.**

### **(c) Characterization of the NbN nanoparticles**

The reaction of NbCl<sub>5</sub> with urea resulted in a silver grey product which gave a XRD pattern shown in Figure 2.13. The pattern is characteristic of cubic NbN (JCPDS = 74-1218) with lattice parameter  $a = 4.44 \text{ \AA}$ .

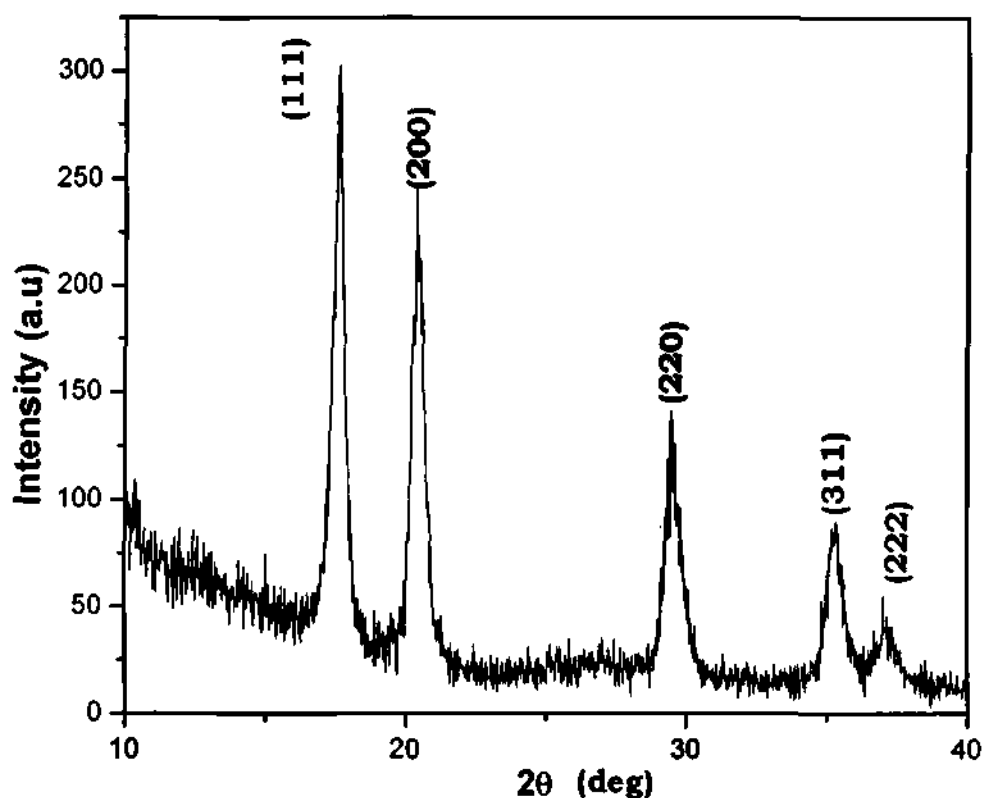


**Figure 2.13: XRD pattern of NbN nanoparticles.**

In Figure 2.14 (a) is shown a SEM image of NbN nanoparticles while the Figure 2.14 (b) gives a TEM image of NbN nanoparticles. The average particle size is around 20 nm which is comparable to that of estimated

from the XRD line widths. The SAED pattern shown in Figure 2.14 (c) is of NbN nanoparticles and it clearly shows the rings corresponding to the (111), (200) and (220) planes. The HREM image of a NbN nanoparticle shown in Figure 2.14 (d) gives a lattice spacing of 0.22 nm corresponding to the (200) planes of NbN.

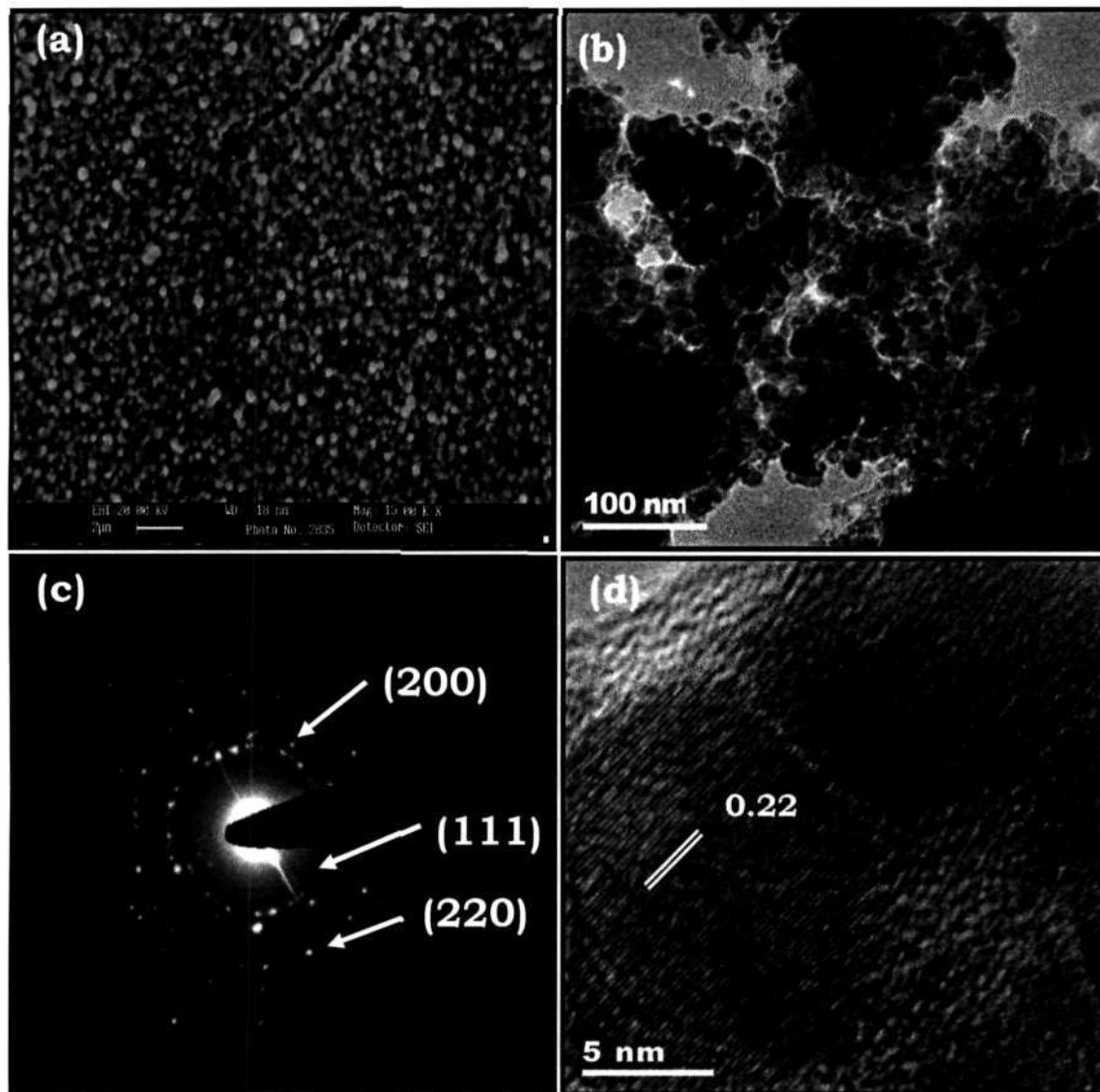


**Figure 2.14: (a) SEM image of the NbN nanoparticles. (b) TEM image of the NbN nanoparticles. (c) SAED pattern of the NbN nanoparticles. (d) HREM image of a NbN nanoparticle.**

We have characterized the NbN nanoparticles by X-ray photoelectron spectroscopy. The XP spectrum of NbN particles in Figure 2.15 gives the BE values of Nb (3d) at 206.7 eV and that of N (1s) at 397 eV.

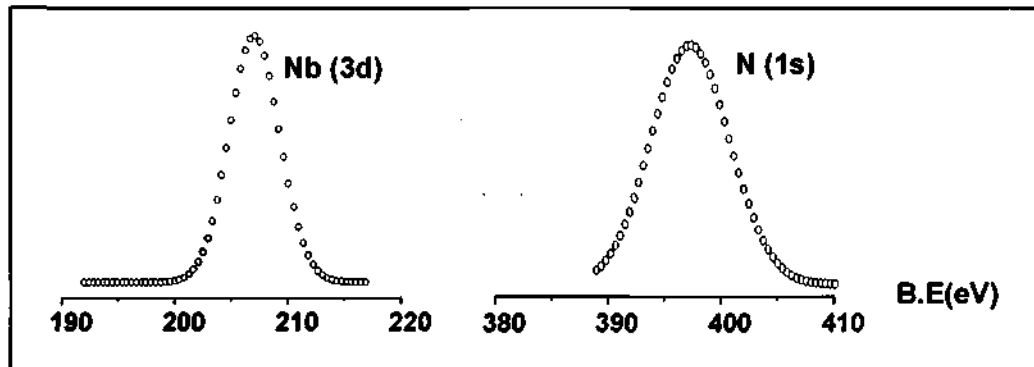


**Figure 2.15: X-ray photoelectron spectrum of NbN.**

In Figure 2.16, we show the results of magnetic measurements on the nanoparticles of NbN under zero-field-cooled (ZFC) condition with the applied field of 5 Oe. The data show a superconducting transition with an onset  $T_c$  around 7 K. The superconducting volume fraction is around 50 %.

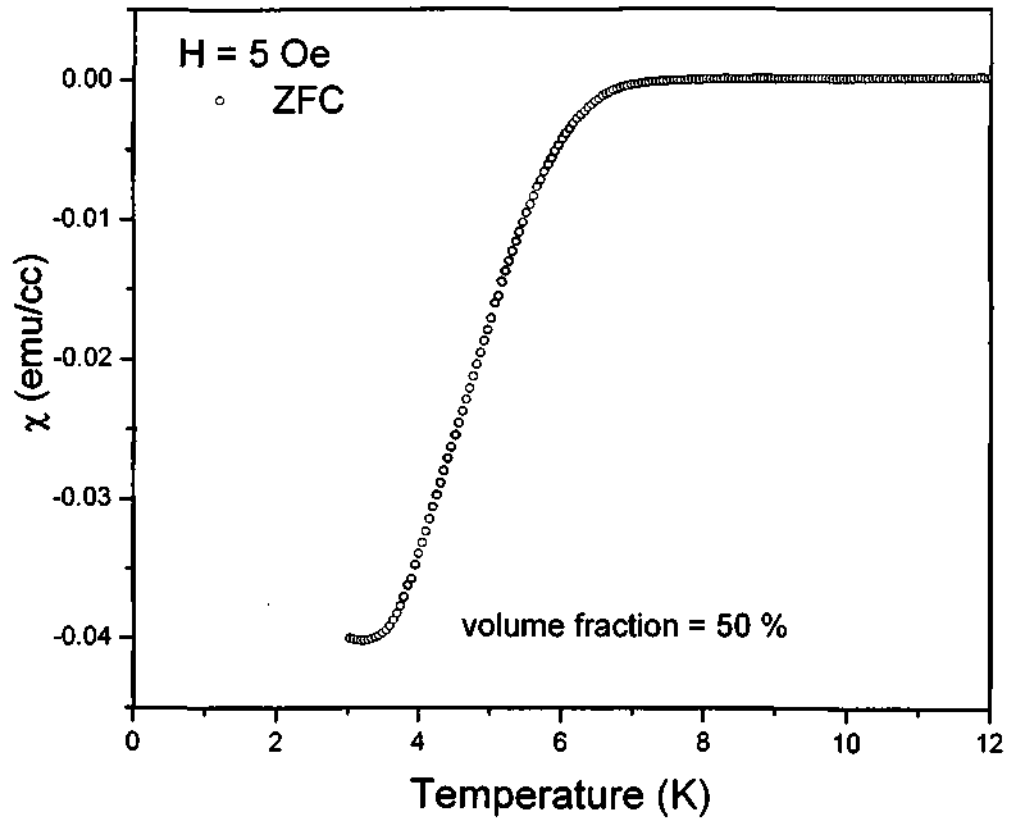


**Figure 2.16: Temperature dependence of magnetic susceptibility of NbN nanoparticles**

## **2.5 Conclusions**

In conclusion, we have succeeded in preparing crystalline nanoparticles of BN, TiN and NbN by heating mixtures of urea with  $\text{H}_3\text{BO}_3$ ,  $\text{TiCl}_4$ , and  $\text{NbCl}_5$  respectively in the temperature range of 900-1273 K. In the case of TiN, nanowires have been obtained by carrying out the reaction of urea with  $\text{TiCl}_4$  over Au islands deposited on Si substrates. The NbN nanoparticles showed a superconducting  $T_c$  around 8 K.

## References

- [1]. R. T. Paine, C. K. Narula, Chem. Rev. 90, 1990, 73.
- [2]. K. P. Loh, M. N. Gamo, I. Sakaguchi, T. Taniguchi, T. Ando, Appl. Phys. Lett. 72, 1998, 3023.
- [3]. K. P. Loh, I. Sakaguchi, M. N. Gamo, T. Sugino, T. Ando, Appl. Phys. Lett. 74, 1999, 28.
- [4]. K. P. Loh, M. N. Gamo, I. Sakaguchi, T. Taniguchi, T. Ando, Diam. Relat. Mater. 8, 1999, 781.
- [5]. L. E. Toth, Transition Metal Carbides and Nitrides, Academic Press, New York, 1971.
- [6]. G. V. Samsonov, I. M. Vinitiskii, Handbook of Refractory Compounds, Academic Press, New York, 1980.
- [7]. R. Buhl, H. K. Pulker, E. Moll, Thin Solid Films, 80, 1981, 265.
- [8]. M. Wittmer, B. Studer, H. Melchior, J. Appl. Phys. 52, 1981, 5722.
- [9]. J. Rivory, J. M. Behaghel, S. Bertier, J. Lafait, Thin Solid Films, 78, 1981, 161.
- [10]. R. A. Andrievski, T. A. Anisomova, V. P. Anisimov, Thin Solid Films, 205, 1991, 171.
- [11]. L. E. Toth, Transition Metal Carbides and Nitrides, Academic Press, New York, 1971.
- [12]. S. T. Oyama, The Chemistry of Transition Metal Carbides and Nitrides, Blackie Academic Professional, Glasgow, 1996.

- [13]. I. Hotovy, D. Buc, J. Brcka, R. Srnanek, *Phys. Stat. Sol.* 161, 1997,97.
- [14]. T. H. Geballe, B. T. Matthias, J. P. remeika, A. M. Glogston, V. B. Compton, J. P. Maita, H. J. Williams, *Physics*, 2, 1966, 293.
- [15]. N. G. Chopra, R. J. Luyken, K. Cherry, V. H. Crespi, M. L. Cohen, S. G. Louie, A. Zettl, *Science*, 269, 1995, 966.
- [16]. P. Cai, L. Chen, L. Shi, Z. Yang, A. Zhao, Y. Gu, T. Huang, Y. Qian, *Solid State Commun.*, 133, 2005, 621.
- [17]. F. L. Deepak, C. P. Vinod, K. Mukhopadhyay, A. Govindaraj, C. N. R. Rao, *Chem. Phys. Lett.* 353, 2002, 345.
- [18]. U. A. Joshi, S. H. Chung, J. S. Lee, *J. Solid State Chem.* 178, 2005, 755.
- [19]. Q. Guo, Y. Xie, X. Wang, S. Lu, T. Hou, C. Bai, *J. Am. Ceram. Soc.*, 88, 2005, 249.
- [20]. X. Feng, Y-J. Bai, B. Lo, C. G. Wang, Y-X. Qi, Y-X. Liu, G-L. Geng, *Inorg. Chem* 43, 2004, 3558.
- [21]. R. A. Janes, M. Aldissi, R. B. Kaner, *Chem. Mater.* 15, 2003, 4431.
- [22]. L. Shi, Y. Gu, L. Chen, Z. Yang, J. Ma, Y. Qian, *J. Nanosci. Nanotech.* 5, 2005, 296.
- [23]. J. Ma, Y. Du, Y. Qian, *Journal of Alloys and Compounds* 389, 2005, 296.
- [24]. S. Podsiadlo, *Thermochim. Acta*, 256, 1995, 367.
- [25]. S. Podsiadlo, *Thermochim. Acta*, 256, 1995, 375.



---

# CHAPTER 3

## Ternary nitrides: Synthesis and characterization\*

---

### Summary

This chapter of the thesis deals with the synthesis of interstitial molybdenum ternary nitrides,  $M_nMo_3N$  ( $M=Fe$  and  $Co$ ,  $n=3$ ;  $M=Ni$ ,  $n=2$ ). For the synthesis of the ternary nitrides the respective molybdates were used as precursors. The nitrides were obtained by heating the molybdate precursors,  $FeMoO_4$ ,  $CoMoO_4$  and  $NiMoO_4$  with urea in the 1:12 molar ratio and heating the mixture in the 1173–1273 K range in a  $N_2$  atmosphere.  $Fe_3Mo_3N$  and  $Co_3Mo_3N$  are obtained in pure form. The nickel nitride has the composition  $Ni_2Mo_3N$  and therefore is in admixture with nickel. The nitrides have been characterized by various physical methods.

---

\* Paper based on this work has been published in Mater. Res. Bull. 2006  
(In Press)

### **3.1 Introduction**

Interstitial ternary nitride materials form an interesting class of compounds. Many of these nitrides are closely allied to the chemistry of their carbides i.e. they have the physical properties of ceramics and electronic properties of metals [1-3]. It is known that they exhibit a number of important properties such as superconductivity [4], catalytic activity [5-7], thermal emissivity [8], unusual magnetic behavior [9-13] and high hardness and strength [14-17] combined with good thermal and electrical conductivity. Ternary molybdenum nitrides constitute examples of promising catalytic materials. They have proved to be active and selective in processes involving hydrogen transfer reactions, such as hydrodenitrogenation and hydrodesulphurization [18]. Recently it has also shown that the catalytic activity of molybdenum nitrides is enhanced by addition of another transition metal like vanadium [19].

### **3.2 Scope of the present study:**

Transition metal-molybdenum ternary nitrides are technologically important class of materials owing to their potential catalytic activity [20]. The ternary interstitial nitrides,  $M_3Mo_3N$  ( $M = Fe, Co$ ) were first synthesized by Bem et al [21] by ammonolysis of oxides and reported to be isostructural to  $\eta\text{-Fe}_3W_3C$ . Another approach to synthesize ternary nitrides of the type  $MWN_2$  ( $M = Fe, Ni, Co$ ) has been to heat the respective

ternary oxide precursor in  $\text{NH}_3$  [22-24]. Weil et al. [25] reported the synthesis of  $\text{Fe}_3\text{Mo}_3\text{N}$ ,  $\text{FeWN}_2$ ,  $\text{Ni}_3\text{Mo}_3\text{N}$  and  $\text{Ti}_3\text{AlN}$  using complex precursors. Synthesis of  $\text{Fe}_3\text{Mo}_3\text{N}$  by the ammonolysis of the oxide precursor has been reported [26]. The ternary nitride,  $\text{Ni}_2\text{Mo}_3\text{N}$ , has been prepared by heating a metalloraganic precursor in  $\text{NH}_3$  [27]. Alconchel et al. [28] have reported a study on the influence of preparative variables on the ammonolysis of the molybdate precursors. Both the ammonolysis as well as the plasma nitridation of  $\text{FeMoO}_4$  and  $\text{CoMoO}_4$  results in the respective intermetallic nitrides [29]. Synthesis of  $\text{Fe}_3\text{Mo}_3\text{N}$  and  $\text{Co}_3\text{Mo}_3\text{N}$  by mechanochemical alloying and by the nitridation of the corresponding ternary carbide has also been reported [30]. Herein we report our investigations on the synthesis of interstitial molybdenum ternary nitrides,  $\text{M}_n\text{Mo}_3\text{N}$  ( $\text{M}=\text{Fe}$  and  $\text{Co}$ ,  $n=3$ ;  $\text{M}=\text{Ni}$ ,  $n=2$ ) by the reaction of the respective ternary metal oxides with urea.

### **3.3 Experimental and related aspects**

#### **(a) Synthesis of oxide precursors:**

The metal molybdates were prepared by the dropwise addition of 400 mL (0.25 M) of an aqueous solution of the metal chloride ( $\text{FeCl}_2$ ,  $\text{CoCl}_2$  or  $\text{NiCl}_2$ ) to a 150-mL (0.55 M)  $\text{Na}_2\text{MoO}_4 \cdot (\text{H}_2\text{O})_2$  solution, and the solution stirred for 2 h to ensure completion of the reaction. The solid product was isolated by vacuum filtration and rinsed with two washings of distilled water followed by a washing with ethanol. The solid was air-dried overnight followed by a drying at 423 K for 24 h. The products were amorphous and had brown, violet and green colors in the case of  $\text{FeMoO}_4$ ,  $\text{CoMoO}_4$  and  $\text{NiMoO}_4$  respectively.

#### **(b) Synthesis of the nitrides:**

To prepare the nitrides, an intimate mixture of the molybdate precursor and urea taken in a molar ratio 1:12 was taken in an alumina boat. The boat was then placed in a quartz tube furnace. Prior to the heat treatment, the furnace was purged with nitrogen for 15 minutes to ensure an inert atmosphere. The molybdate-urea mixture was then heated at 1173 K for 3 h in a  $\text{N}_2$  atmosphere. In the case of all nitrides the product obtained was black in color.

### **(c) Characterization Techniques:**

**X-ray Diffraction:** X-ray diffraction (XRD) patterns of the nitrides were recorded using Cu K $\alpha$  radiation on a Rich-Siefert XRD-3000-TT diffractometer.

**Scanning electron microscopy:** Scanning electron microscope (SEM) micrographs were obtained using a LEICA S440i SEM.

**Mössbauer Spectroscopy:** The Mössbauer spectrum was recorded using a Wissel spectrometer. The spectrum was recorded at room temperature using a  $^{57}\text{Co}$  source. The sampling was done by making a pellet of the nitride with polyethylene as the matrix. The isomer shift is reported relative to metallic iron at room temperature.

**Electrical resistivity measurements:** Electrical resistivity of the nitride samples were measured using four probe technique from 50 to 300 K.

### **3.4 Results and Discussions:**

#### **(a) Characterization of the Fe<sub>3</sub>Mo<sub>3</sub>N:**

The product obtained by heating a mixture of FeMoO<sub>4</sub> with urea in a 1:12 molar ratio gave a XRD pattern given in Figure 3.1. The XRD pattern confirms the formation of Fe<sub>3</sub>Mo<sub>3</sub>N. The pattern could be indexed with the space group *Fd3m* (JCPDS card no: 48-1408) with a lattice parameter of  $a = 11.0620 \text{ \AA}$ . Fe<sub>3</sub>Mo<sub>3</sub>N adopts a pattern similar to that of the cubic *eta* carbide  $\eta\text{-Fe}_3\text{W}_3\text{C}$ . The structure consists of NMo<sub>6</sub> octahedra that are corner shared, with the iron atoms occupying the sites between the octahedra. The iron atoms are located in 12-fold, pseudo-icosahedral coordination, surrounded by six molybdenum and six iron atoms, or four molybdenum, two nitrogen, and six iron atoms to give Fe-[Mo<sub>6</sub>Fe<sub>6</sub>] and Fe[Mo<sub>6</sub>Fe<sub>4</sub>N<sub>2</sub>].

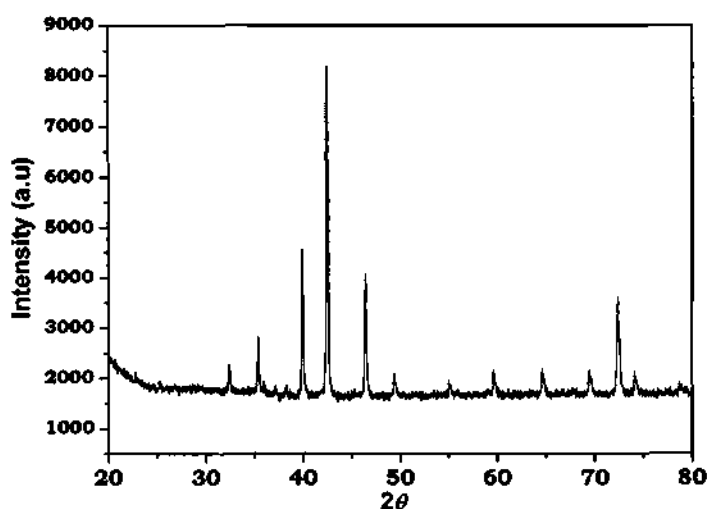


**Figure 3.1: XRD pattern of Fe<sub>3</sub>Mo<sub>3</sub>N**

We show the Mössbauer spectrum of  $\text{Fe}_3\text{Mo}_3\text{N}$  recorded at room temperature in Figure 3.2.

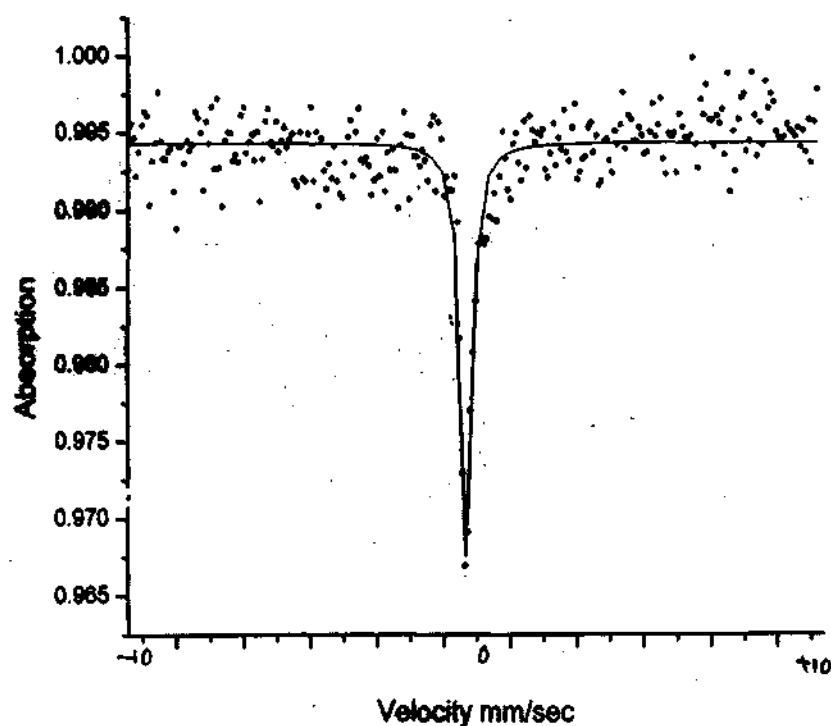


**Figure 3.2: Mössbauer spectrum of  $\text{Fe}_3\text{Mo}_3\text{N}$ .**

The spectrum shows a symmetric single line with an isomer shift of  $0.213 \text{ mm s}^{-1}$  characteristic of  $\text{Fe}_3\text{Mo}_3\text{N}$  as reported in the literature [31]. Mössbauer results give the distribution of iron sites. The isomer shift value,  $0.213 \text{ mm s}^{-1}$ , is very close to that of the alloys of  $\text{Al}-(\text{Mn}_{0.7}\text{Fe}_{0.3})$  whose isomer shift value is  $0.22 \text{ mm s}^{-1}$ . This suggests that, as in the case of icosahedral alloys, in  $\text{Fe}_3\text{Mo}_3\text{N}$  the Fe atoms are located in 12 fold, pseudo-icosahedral coordination surrounded by six Mo and six Fe

atoms or six Mo, two N and four Fe atoms. That is the structure of  $\text{Fe}_3\text{Mo}_3\text{N}$  has iron atoms occupying the sites between the  $(\text{NMo}_6)$  octahedra which are corner-shared. The product consisted of sub-micrometer sized particles as revealed by the SEM image shown in Figure 3.3 (a).

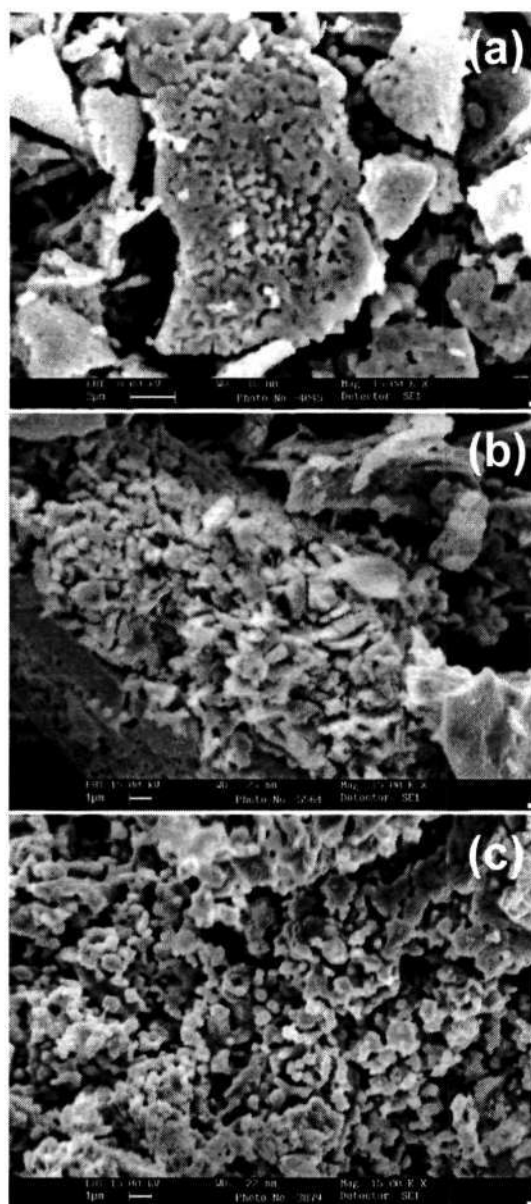


**Figure 3.3: SEM images of (a)  $\text{Fe}_3\text{Mo}_3\text{N}$  (b)  $\text{Co}_3\text{Mo}_3\text{N}$  (c)  $\text{Ni}_2\text{Mo}_3\text{N}$ .**



### **(a) Characterization of the $\text{Co}_3\text{Mo}_3\text{N}$ :**

By heating a 1:12 mixture of  $\text{CoMoO}_4$  and urea, we obtained  $\text{Co}_3\text{Mo}_3\text{N}$  showing a XRD pattern characteristic of cubic eta carbide structure as shown in the Figure 3.4. The pattern could be indexed with the space group  $Fd3m$  with a cell parameter of 11.0134 Å.

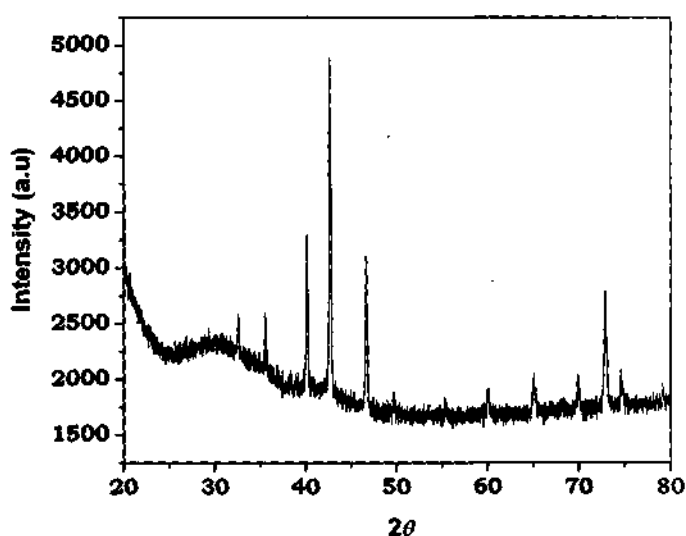


**Figure 3.4: XRD pattern of  $\text{Co}_3\text{Mo}_3\text{N}$**

The product consisted of sub-micrometer sized particles as revealed by the SEM image in Figure 3.3 (b). The nitride was metallic as shown by the measurement of the temperature variation of resistivity in Figure 3.5.

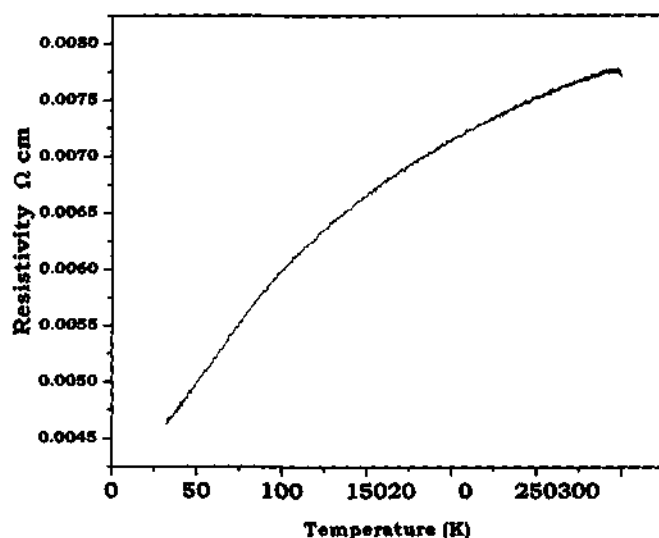


**Figure 3.5: Variation of resistivity,  $\rho$ , of  $\text{Co}_3\text{Mo}_3\text{N}$  with temperature**

The reactions involved in the formation of  $\text{Fe}_3\text{Mo}_3\text{N}$  and  $\text{Co}_3\text{Mo}_3\text{N}$  is likely to be (1):



Here,  $\text{NH}_3$  is generated by the decomposition of urea.

### **(a) Characterization of the $\text{Ni}_2\text{Mo}_3\text{N}$ :**

The product of heating a mixture of  $\text{NiMoO}_4$  and urea in the molar ratio 1:12 resulted in a mixture of  $\text{Ni}_2\text{Mo}_3\text{N}$  and Ni which is ascertained by the XRD pattern given in Figure 3.6. Unlike the ternary nitrides of iron and cobalt which forms the nitrides of type  $\text{M}_3\text{Mo}_3\text{N}$  which adopts a structure similar to that of eta carbide, the nickel molybdenum ternary nitride forms  $\text{Ni}_2\text{Mo}_3\text{N}$  which has a structure

similar to that of  $\text{Al}_2\text{Mo}_3\text{C}$  which adopts filled  $\beta$ -Mn structure. The pattern could be indexed with the space group  $P4_32$  with a lattice parameter  $a = 6.9001 \text{ \AA}$  and reveals the presence of nickel impurity as required by the reaction (2).

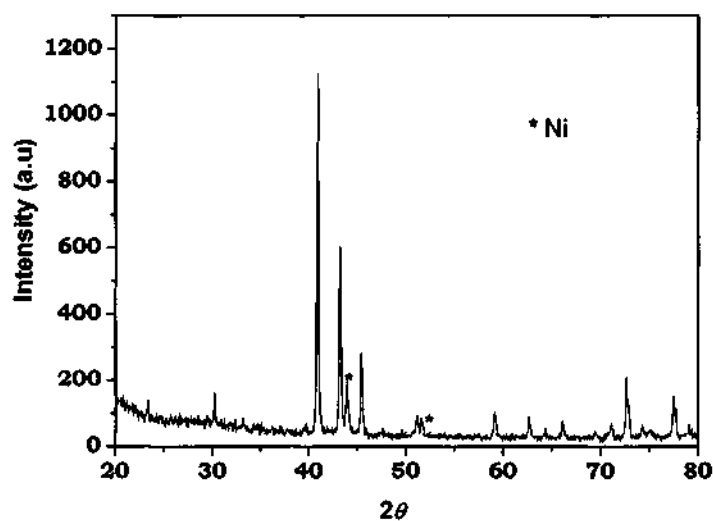


**Figure 3.6: XRD pattern of  $\text{Ni}_2\text{Mo}_3\text{N}$**

In Figure 3.3 (c) we show the SEM image of the product obtained by heating the nickel molybdate-urea mixture, which reveals the morphology of product to be sub-micrometer sized particles. The presence of nickel was ascertained by magnetic measurements which showed ferromagnetism.

### **3.5 Conclusions**

In conclusion, we have been able to prepare three ternary nitrides of type  $M_nMo_3N$  ( $n=3$  with  $M=Fe$  and  $Co$  and  $n=2$  with  $M=Ni$ ) by a simple reaction of the precursor molybdates with urea. All the nitrides were of sub-micron sized particles as revealed by the SEM micrographs.

## References

- [1]. Z. Altouninan, X. Chen, L. X. Liao, D. H. Ryan, J. O. Strom-Olsen, *J. Appl. Phys.*, 73, 1993, 6017.
- [2]. S. T. Oyama, *J. Solid State Chem.*, 96, 1992, 442.
- [3]. S. T. Oyama (ed.), *The Chemistry of Transition Metal Carbides and Nitrides*, Blackie Academic, London, 1996.
- [4]. F. J. DiSalvo, *Science*, 247, 1990, 649.
- [5]. L. Volpe, M. Boudart, *J. Solid State Chem.*, 59, 1985, 332.
- [6]. R. B. Levy, M. Boudart, *Science*, 181, 1973, 547.
- [7]. L. Volpe, M. Boudart, *Catal. Rev. Sci. Eng.*, 27, 1985, 515.
- [8]. A. J. Perry, M. Georgson, W. D. Sproul, *Thin Solid Films*, 157, 1988, 255.
- [9]. K. H. J. Buschow, R. Coehoorn, D. B. de Mooij, K. de Waard, T. H. Jacobs, *J. Magn. Magn. Mater.* 92, 1990, 35.
- [10]. Y. Otani, D. P. F. Hurley, H. Sun, J. M. D. Coey, *J. Appl. Phys.*, 69, 1991, 5584.
- [11]. S. Miraglia, J. L. Soubeyroux, C. Kolbeck, O. Ishard, D. Fruchart, M. Guillot, *J. Less-Common Met.*, 171, 1991, 51.
- [12]. D. P. F. Hurley, H. Sun, J. M. D. Coey, *J. Magn. Magn. Mater.* 99, 1991, 229.
- [13]. H. J. Buschow, *J. Magn. Magn. Mater.* 100, 1991, 79.
- [14]. M. Y. Chern, F. J. DiSalvo, *J. Solid State Chem.*, 88, 1990, 459.

- [15]. L. E. Toth, *Transition Metal Carbides and Nitrides*, Academic Press, New York, 1971.
- [16]. H. Randhawa, P. C. Johnson, R. Cunningham, *J. Vac. Sci. Technol. A6*, 1988, 2136.
- [17]. U. Konig, *Surf. Coat Technol.*, 33, 1987, 91.
- [18]. C. H. Jagers, J. N. Michaels, A. M. Stacy, *Chem. Mater.*, 2, 1990, 150.
- [19]. C. C. Yu, S. T. Oyama, *J. Solid State Chem.*, 116, 1995, 207.
- [20]. C. J. H. Jacobsen, *Chem. Commun.*, 2000, 1057.
- [21]. D. S. Bem, C. P. Gibson, H.-C.zur Loye, *Chem. Mater.*, 5, 1993, 397.
- [22]. J. D. Houmes, S. Deo, H.-C.zur Loye, *J. Solid State Chem.* 131, 1997, 374.
- [23]. P.S. Herle, N. Y. Vasanthacharya, M. S. Hegde, J. Gopalakrishnan, *Journal of Alloys and Compounds* 217, 1995, 22.
- [24]. D. S. Bem, H.-C.zur Loye, *J. Solid State Chem.* 104, 1993, 467.
- [25]. K. S. Weil, P. N. Kumta, *Materials Science and Engineering B* 38, 1996, 109.
- [26]. R. N. Panda, N. S. Gajbhiye, *Journal of Alloys and Compounds* 256, 1997, 102.
- [27]. P.S. Herle, M. S. Hegde, K. Sooryanarayana, T. N. Guru Row, G. N. Subbanna, *Inorg. Chem.* 37, 1998, 4128.

- [28]. S. Alconchel, F. Sapiña, D. Beltrán, A. Beltrán, *J. Mater. Chem.*, 8, 1998, 1901.
- [29]. S. K. Jackson, R. C. Layland, H.-C.zur Loye, *Journal of Alloys and Compounds*, 291, 1999, 94.
- [30]. C. J. H. Jacobsen, J. J. Zhu, H.Lindeløv, J. Z. Jiang, *J. Mater. Chem.*, 12, 2002, 3113.
- [31]. R. N. Panda, N. S. Gajbhiye, *Journal of Alloys and Compounds* 256, 1997, 102.

---

---

# **CHAPTER 4**

## **Superconducting molybdenum nitrides: Synthesis and characterization\***

---

---

### **Summary**

This chapter of the thesis deals with the preparation of the nanoparticles (~ 4 nm diameter) of cubic  $\gamma$ -Mo<sub>2</sub>N by a simple procedure involving the reaction of MoCl<sub>5</sub> with urea at 873 K. The nanoparticles show a superconducting transition around 6.5 K. The  $\gamma$ -Mo<sub>2</sub>N nanoparticles are readily transformed to nanoparticles of  $\delta$ -MoN with a slightly larger diameter on heating in a NH<sub>3</sub> atmosphere at 573 K. Phase-pure  $\delta$ -MoN obtained by this means shows a superconducting transition around 5 K. The nanoparticles of  $\gamma$ -Mo<sub>2</sub>N and  $\delta$ -MoN exhibit magnetic hysteresis at 300 K as a surface property, just as the nanoparticles of many oxides.

---

\* Paper based on this work has been published in Journal of Solid State Chemistry (ASAP).



## **4.1 Introduction:**

Transition metal nitrides have attracted scientific attention because of their often unusual electrical, magnetic, chemical and mechanical properties which is exhibited due to the nature of their chemical bonds [1-3]. Especially molybdenum nitrides, as materials with significant catalytic properties, have gained growing interest. There has been an increasing number of reports on molybdenum nitrides as heterogeneous catalysts for several hydrotreating reactions in petrochemical process [4], ammonia synthesis [5], ethane hydrogenolysis [6], carbon monoxide hydrogenation [7] and catalytic decomposition of hydrazine in satellite microthrusters [8]. At the same time, nitrides of molybdenum are well known as superconductors with superconducting properties retained over a wide range of nitrogen composition. Molybdenum nitride phases known to-date include the stoichiometric, hexagonal compound  $\delta$ -MoN, and two nonstoichiometric compounds, cubic  $\gamma$ -Mo<sub>2</sub>N and tetragonal  $\beta$ -Mo<sub>2</sub>N.  $\delta$ -MoN is a hard material with a low compressibility, showing a superconducting transition in the 4-12 K range [9-10].  $\gamma$ -Mo<sub>2</sub>N is also known to be a superconductor with a  $T_c$  of 5.2 K [11]. A theoretical study has predicted that  $\gamma$ -MoN with a cubic NaCl type structure would have a superconducting  $T_c$  as high as 29 K [12].

## **4.2 Scope of the present study:**

Identification of  $\gamma$ -Mo<sub>2</sub>N as a catalytic material has led to considerable research efforts directed towards its synthesis. Most of the work reported has involved synthesizing the material by reacting the oxide with NH<sub>3</sub> at elevated temperatures. A process that has received much attention is the temperature programmed reaction of MoO<sub>3</sub> with NH<sub>3</sub> [13]. Other than this following are some of the methods by which molybdenum nitrides are synthesized. Lengauer [14] has investigated the formation of  $\gamma$ -Mo<sub>2</sub>N and  $\delta$ -MoN by the reaction between MoCl<sub>5</sub> and ammonia while Bull et al. [10] obtained phase-pure  $\delta$ -MoN by this reaction carried out at 933 K. Marchand et al. [15] obtained powders of  $\delta$ -MoN and Mo<sub>5</sub>N<sub>6</sub> by the ammonolysis of MoS<sub>2</sub>. Nanocrystalline  $\gamma$ -Mo<sub>2</sub>N and  $\delta$ -MoN with  $T_c$  values of 3.8 K and 7.5 K respectively, have been prepared by heating hydroxylamine complexes of molybdenum in NH<sub>3</sub> [16].

We have developed a very simple method to prepare  $\gamma$ -Mo<sub>2</sub>N and  $\delta$ -MoN by employing the urea route based on the reaction of metal halides with urea. By employing the reaction of MoCl<sub>5</sub> with urea we have obtained nanoparticles of  $\gamma$ -Mo<sub>2</sub>N. By heating  $\gamma$ -Mo<sub>2</sub>N in a NH<sub>3</sub> atmosphere, we were able to prepare stoichiometric  $\delta$ -MoN. Both  $\gamma$ -Mo<sub>2</sub>N and  $\delta$ -MoN prepared by us are in nanoparticulate form, exhibiting superconductivity.

### **4.3 Experimental and related aspects:**

#### **(a) Synthesis of nitrides:**

For the synthesis of  $\gamma$ -Mo<sub>2</sub>N a mixture of MoCl<sub>5</sub> and urea taken in the molar ratio 1:12 was heated at 873 K in an inert atmosphere. In a typical reaction 0.273 g of MoCl<sub>5</sub> was mixed with 0.720 g of urea. The mixture was then placed in an alumina boat and heated at 873 K in a quartz tube furnace for 3h in a N<sub>2</sub> atmosphere. The product obtained was black powder. Alternatively a molybdenum-urea complex can be used to synthesize  $\gamma$ -Mo<sub>2</sub>N. For 0.273 g of MoCl<sub>5</sub> dissolved in acetonitrile about 0.720 g of urea in acetonitrile was added and the solution was stirred for 2h to ensure the completion of the reaction. At the end of 2h a brown precipitate was formed. The precipitate was taken in an alumina boat and heated at 873 K for 3h in a nitrogen atmosphere which resulted in a black powder.  $\delta$ -MoN was synthesized by heating  $\gamma$ -Mo<sub>2</sub>N obtained by the above reaction in NH<sub>3</sub> atmosphere for 72h.

#### **(b) Characterization Techniques:**

**X-ray Diffraction:** X-ray diffraction (XRD) patterns of the nitrides were recorded using Cu K $\alpha$  radiation on a Rich-Siefert XRD-3000-TT diffractometer.

**Scanning electron microscopy:** Scanning electron microscope (SEM) images were obtained using a LEICA S440i SEM.

**Transmission electron microscopy:** For transmission electron microscopy, the nitrides were dispersed in  $\text{CCl}_4$  and dropped on to the holey carbon-coated copper grids. The grids were allowed to dry in the air. Transmission electron microscope (TEM) images were obtained with a JEOL JEM 3010, operating with an accelerating voltage of 300 kV.

**Thermogravimetric analysis:** Thermogravimetric analysis (TGA) was carried out on a Mettler-Toledo-TG-850 instrument.

**Magnetic properties:** Magnetic measurements of the as-prepared powder samples were carried out with a vibrating sample magnetometer in Physical Property Measurements System (PPMS, Quantum Design).

## **4.4 Results and Discussions:**

### **(a) Characterization of the $\gamma\text{-Mo}_2\text{N}$ nanoparticles:**

The product of heating the 1:12 mixture of  $\text{MoCl}_5$  and urea at 873 K for 3 h gave the XRD pattern shown in Figure 4.1. The pattern is characteristic of cubic  $\gamma\text{-Mo}_2\text{N}$ .

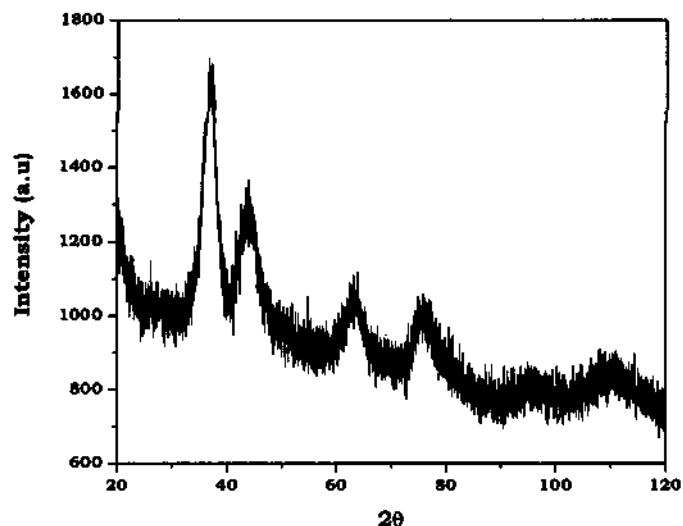


**Figure 4.1: XRD pattern of  $\gamma$ -Mo<sub>2</sub>N**

The pattern could be indexed with the space group Pm3m (JCPDS card no: 25-1366) with a lattice parameter  $a = 4.1497 \text{ \AA}$ . Based on the line widths by making use of Scherrer formula we estimated the particle size to be  $\sim 6 \text{ nm}$ .

The TEM image shown in Figure 4.2 (a) is that of as-prepared  $\gamma$ -Mo<sub>2</sub>N nanoparticles. From the TEM image it is evident that the particles are agglomerated. The SAED pattern shown as inset of Figure 4.2 (a) shows rings corresponding to (111) and (200) planes. When the as-prepared  $\gamma$ -Mo<sub>2</sub>N nanoparticles were sonicated in CCl<sub>4</sub> for 15 minutes they dispersed as evidenced by the TEM image shown in Figure 4.2 (b). From TEM image we calculated the average particle size to be  $\sim 4.5 \text{ nm}$  as seen by the histogram given as an inset. The SAED pattern shown as an

inset in Figure 4.2 (b) gives spots corresponding to the (111) and (200) planes of  $\gamma$ - $\text{Mo}_2\text{N}$ .

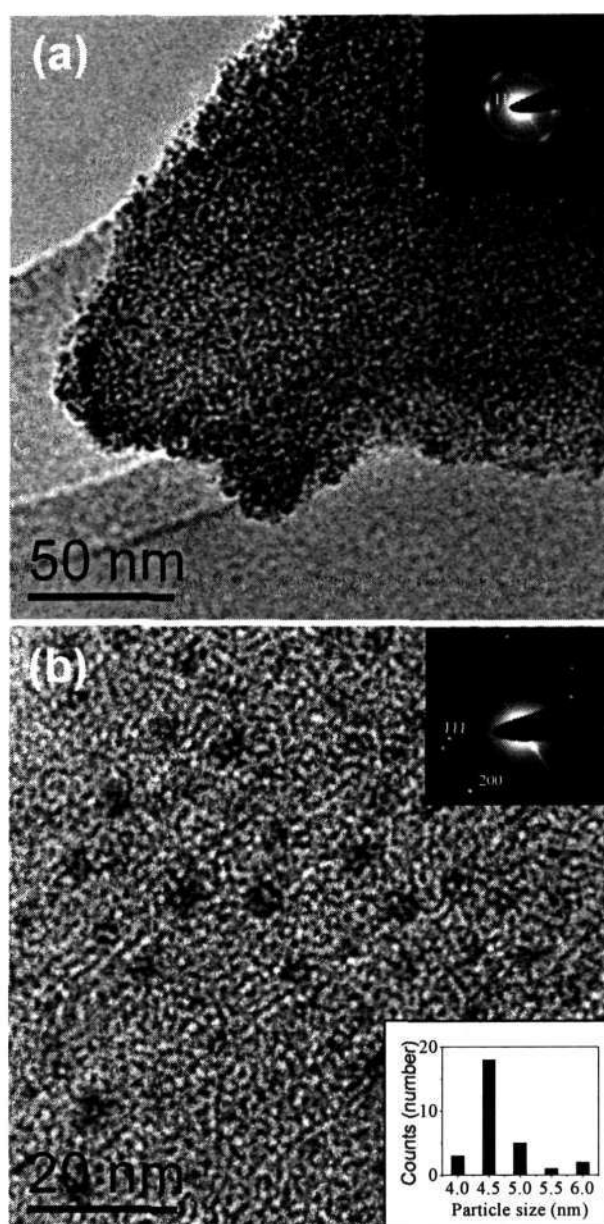


**Figure 4.2: (a) TEM image of the as-synthesized  $\gamma$ - $\text{Mo}_2\text{N}$  particles and the inset shows the SAED pattern of the particles (b) TEM image of the  $\gamma$ - $\text{Mo}_2\text{N}$  particles sonicated for 15 minutes with the inset showing the SAED pattern of a particle.**

In order to calculate the stoichiometry of the  $\gamma$ -Mo<sub>2</sub>N we carried out the TGA of the same in an oxygen atmosphere. In Figure 4.3 is given the TGA curve of the  $\gamma$ -Mo<sub>2</sub>N carried out in oxygen atmosphere. The initial increase in mass is due to oxidation reaction. As per the mass loss, the final product corresponds to MoO<sub>3</sub>. The XRD pattern of the product, shown as an inset in Figure 4.3, confirms the product to be MoO<sub>3</sub>. The stoichiometry of the nitride calculated from TGA is MoN<sub>0.56</sub>.

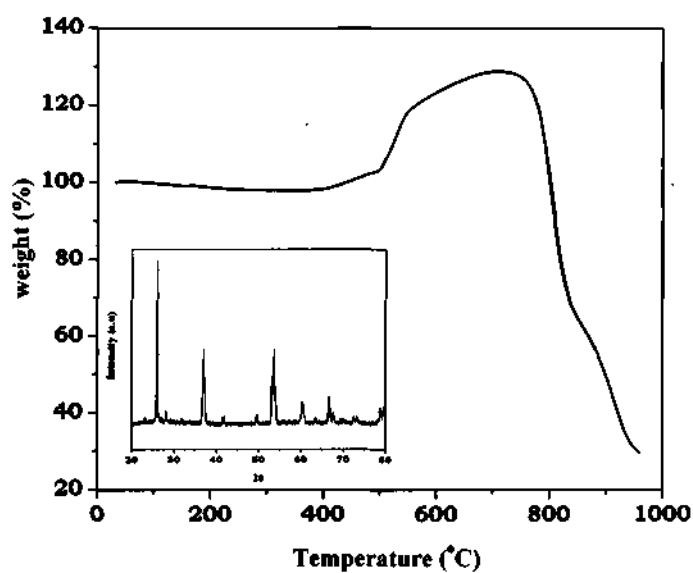


**Figure 4.3: TGA of  $\gamma$ -Mo<sub>2</sub>N in oxygen atmosphere with inset showing the XRD pattern of the final product recorded using Cu K $\alpha$  radiation.**

From the literature it is known that  $\gamma\text{-Mo}_2\text{N}$  is known to be a superconductor with a  $T_c$  of 5.2 K [9]. In Figure 4.4, we show the results of magnetic measurements on the nanoparticles of  $\gamma\text{-Mo}_2\text{N}$  under zero-field-cooled (ZFC) conditions (at 19.6 Oe).

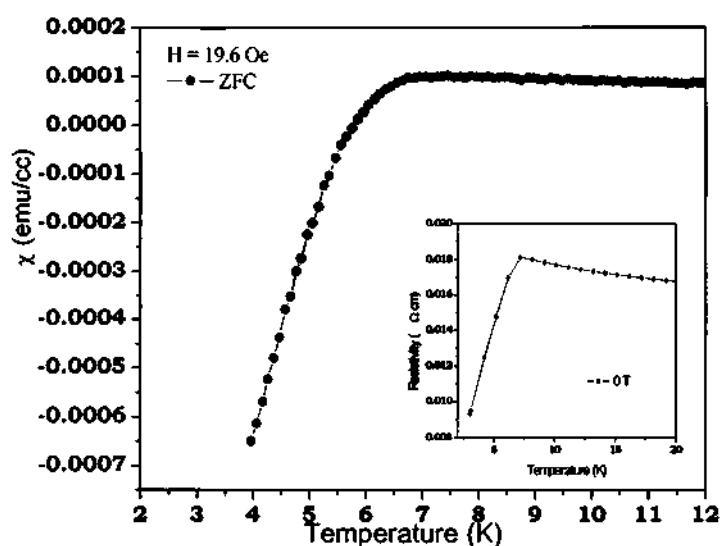


**Figure 4.4: Temperature dependence of magnetic susceptibility of  $\gamma\text{-Mo}_2\text{N}$  nanoparticles with the inset showing resistivity of the sample as a function of temperature.**

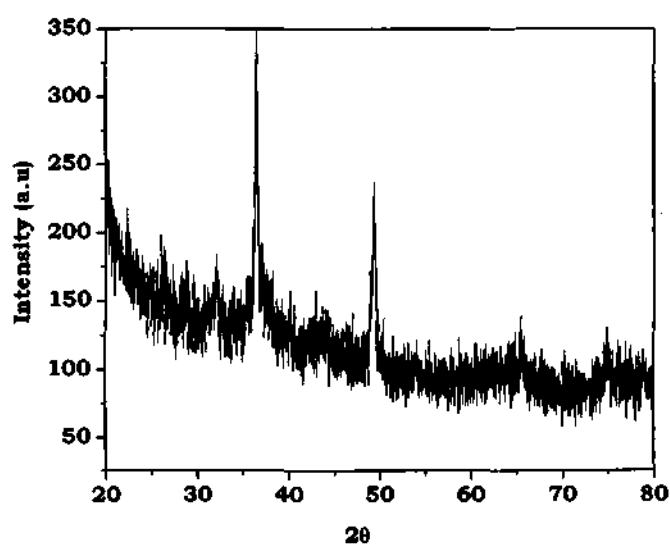
The data show a superconducting transition with an onset  $T_c$  around 6.5 K. Electrical resistivity measurements on the  $\gamma\text{-Mo}_2\text{N}$  nanoparticles (shown as an inset in Fig. 4) shows the superconducting transition with a  $T_c$  of around 7 K. The superconducting volume fraction is around 0.8



%. It is noteworthy that the nanoparticles of  $\gamma$ -Mo<sub>2</sub>N with an average size of 4.5 nm exhibit superconductivity.

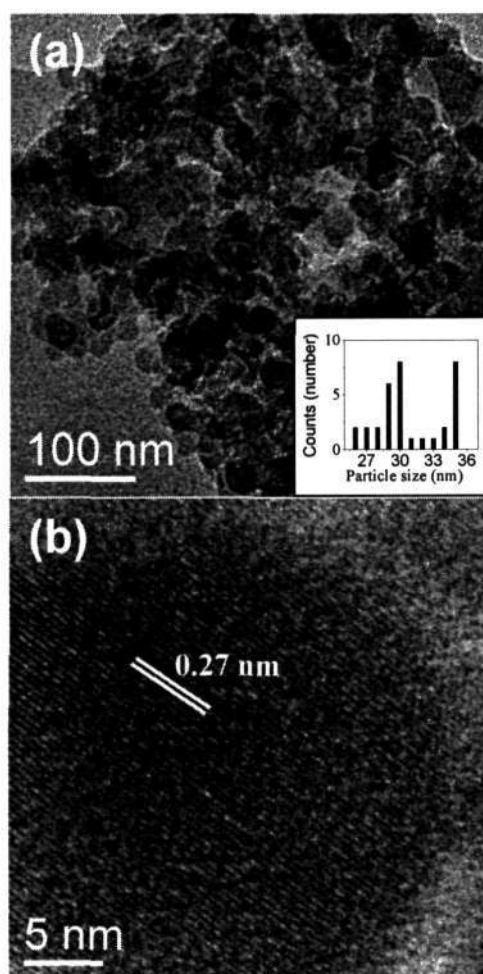
**(a) Characterization of the  $\delta$ -MoN nanoparticles:**

In order to prepare  $\delta$ -MoN, we heated the 4.5 nm nanoparticles of  $\gamma$ -Mo<sub>2</sub>N in a NH<sub>3</sub> atmosphere for 72 h at 573 K. The product gave the XRD pattern characteristic of  $\delta$ -MoN as shown in Figure 4.5. It has a hexagonal structure of space group P6<sub>3</sub>/mmc with  $a = 5.68 \text{ \AA}$ ,  $c = 5.56 \text{ \AA}$  (JCPDS card no: 25-1367). Based on the XRD line-widths, the particle size is estimated to be ~40 nm.



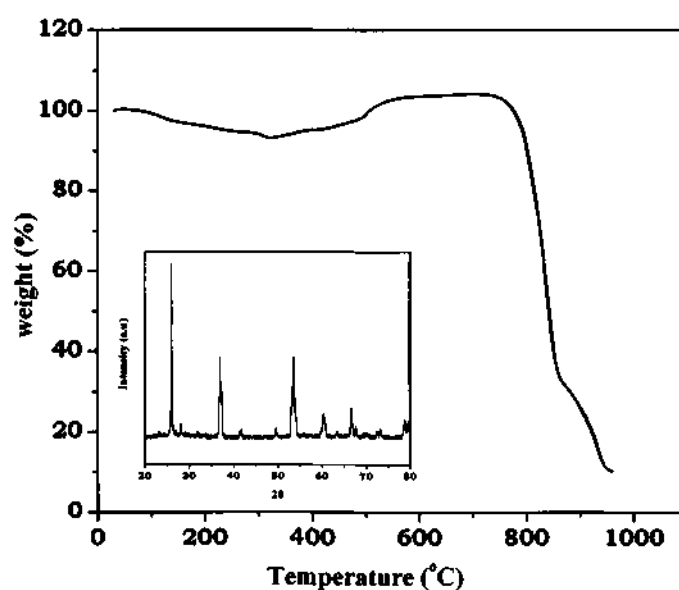
**Figure 4.5: XRD pattern of  $\delta$ -MoN**

Figure 4.6(a) shows the TEM image of the  $\delta$ -MoN nanoparticles. From the TEM image, we estimate the particle size to be in the 30-35 nm range. It appears that the  $\gamma$ -Mo<sub>2</sub>N to  $\delta$ -MoN transformation in an NH<sub>3</sub> atmosphere is accompanied by an increase in particle size. The high resolution electron microscope (HREM) image in Figure 4.6(b) reveals the nanoparticles to be single crystalline. It is interesting that single crystalline  $\gamma$ -Mo<sub>2</sub>N transforms to single crystalline  $\delta$ -MoN.



**Figure 4.6: (a) TEM image of the  $\delta$ -MoN nanoparticles (b) HREM image of a  $\delta$ -MoN particle.**

The TGA curve of  $\delta$ -MoN carried out in an oxygen atmosphere is shown in Fig. 4.7. The TGA curve gave a mass loss corresponding to the formation of  $\text{MoO}_2$  as confirmed by the XRD pattern of the product. Here again, the initial increase in mass is due to the oxidation reaction and the calculated stoichiometry of the nitride from TGA is  $\text{MoN}_{0.95}$ .



**Figure 4.7: TGA of  $\delta$ -MoN in oxygen atmosphere with inset showing the XRD pattern of the final product recorded using  $\text{Cu K}\alpha$  radiation.**

We tried to prepare  $\delta$ -MoN by the reaction of  $\gamma$ -Mo<sub>2</sub>N with urea, but always ended with a slightly impure product. This is because when urea is decomposed at relatively low temperatures, there will be other side-products in addition to one mole of NH<sub>3</sub> for one mole of urea. The side products can be eliminated at high temperatures but under those conditions  $\delta$ -MoN is not stable.

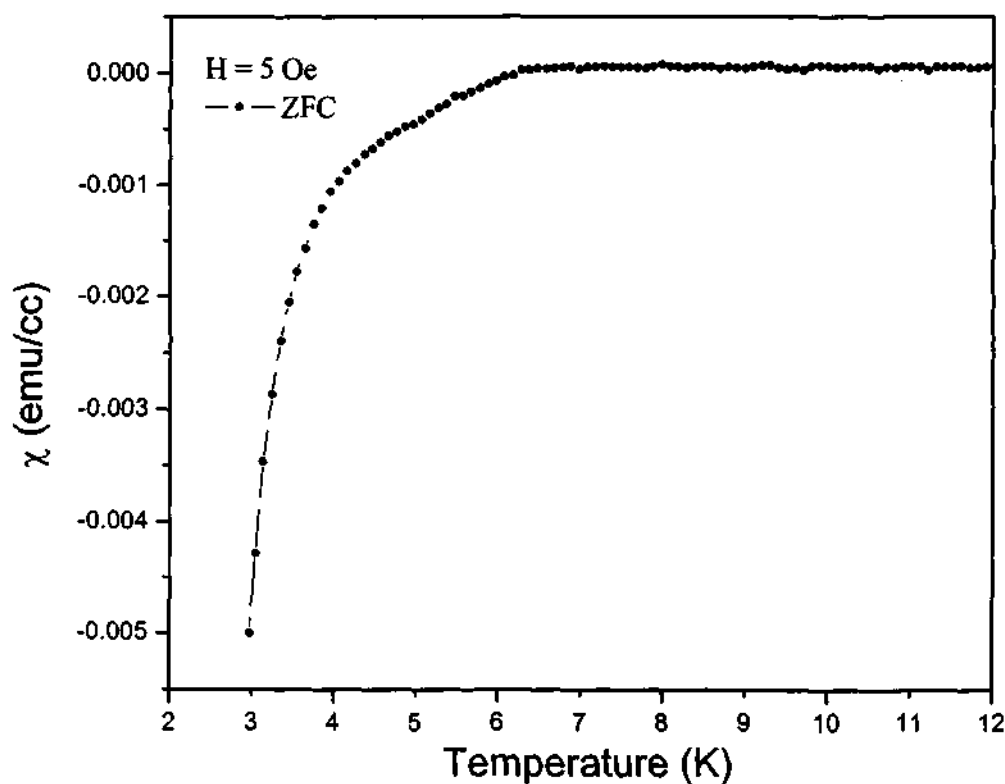


**Figure 4.8: Temperature dependence of magnetic susceptibility of  $\delta$ -MoN nanoparticles.**

It is known that  $\delta$ -MoN is a hard material with a low compressibility, showing a superconducting transition in the 4-12 K range [10,11]. In Figure 4.8, we show the results of magnetic measurements on the nanoparticles of  $\delta$ -MoN under zero-field-cooled (ZFC) conditions (at 5 Oe). We see a superconducting transition around 5.6 K. The superconducting volume fraction is around 6.3 %. It is known that the superconducting transition temperature of  $\delta$ -MoN varies with the extent of disorder in the structure, the  $T_c$  of 4 K in highly disordered  $\delta$ -MoN increasing to a value of 12.1 K in the ordered phase [11]. The  $T_c$  observed by us is in between these values.

#### **4.5 Ferromagnetism in nanoparticles:**

While the existence of ferromagnetism in transition metal-doped semiconducting oxides remains controversial [17], thin films of the band insulator HfO<sub>2</sub> have been reported to exhibit ferromagnetism at room temperature in the absence of any doping [18]. This is puzzling, since pure HfO<sub>2</sub> does not have any magnetic moment and the bulk sample is diamagnetic. Similar ferromagnetism has been reported in other nonmagnetic materials such as CaB<sub>6</sub>, CaO, and SiC where the origin of ferromagnetism is believed to be due to intrinsic defects [19-21]. It has been suggested that ferromagnetism in thin films of HfO<sub>2</sub> may be related to anion vacancies [22]. It has been reported very recently that thin films as well as nanoparticles of several metal oxides show ferromagnetism at

room temperature, the corresponding bulk forms of these materials being diamagnetic [23,24]. Thin films of these oxides might have defects or oxygen vacancies that could be responsible for the observed ferromagnetism. Herein we have investigated the ferromagnetism exhibited by the nanoparticles of superconducting  $\gamma$ -Mo<sub>2</sub>N,  $\delta$ -MoN and NbN prepared by the urea route.

Nanoparticles of  $\gamma$ -Mo<sub>2</sub>N of ~4.5 nm in size were prepared by heating a mixture of MoCl<sub>5</sub> and urea taken in the molar ratio 1:12 at 873 K in an inert atmosphere. The  $\gamma$ -Mo<sub>2</sub>N nanoparticles so obtained was heated in NH<sub>3</sub> atmosphere for 72 h to give  $\delta$ -MoN. The average particle size of  $\delta$ -MoN nanoparticles was 30-35 nm. NbN nanoparticles of ~20 nm were prepared by heating a 1:12 mixture of NbCl<sub>5</sub> and urea at 1173 K for 3 h in a N<sub>2</sub> atmosphere.

In Figure 4.9 we show the magnetization-field curve of  $\gamma$ -Mo<sub>2</sub>N nanoparticles. It is seen from the M(H) curve that the nanoparticles show ferromagnetic behavior. The  $\gamma$ -Mo<sub>2</sub>N nanoparticles show a superconducting transition with a  $T_c$  around 6.5 K. This is shown as inset in the Figure 4.9. In Figure 4.10 is shown the magnetization-field curve of  $\delta$ -MoN nanoparticles with the inset showing the superconducting transition with a  $T_c$  around 5.6 K

Having found magnetic hysteresis in nanoparticles of MoN<sub>x</sub>, we attempted to see if this behavior is found in nanoparticles of other nitride superconductors.

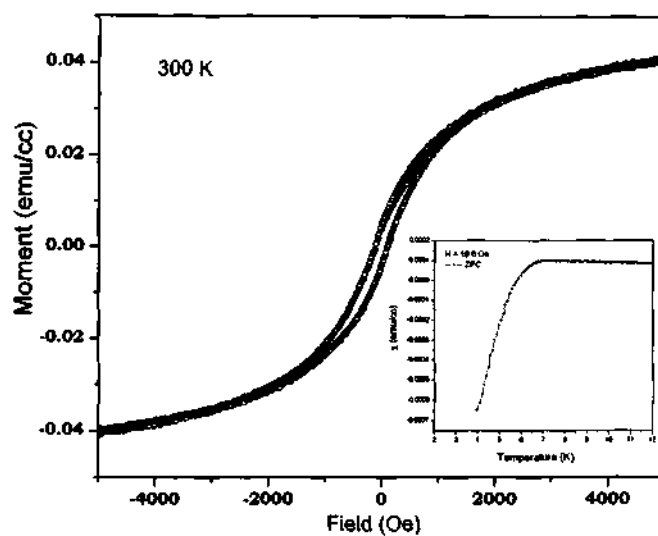


**Figure 4.9: Magnetization curve of  $\gamma$ -Mo<sub>2</sub>N nanoparticles at 300 K with the inset showing the superconducting transition of the same at ~6.5 K**

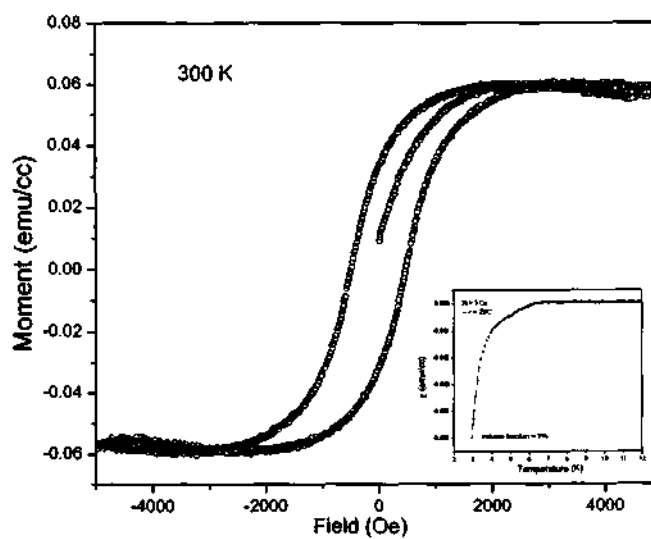


**Figure 4.10: Magnetization curve of  $\delta$ -MoN nanoparticles at 300 K with the inset showing the superconducting transition of the same at ~6 K**

We found that NbN nanoparticles of ~20 nm in diameter with a superconducting transition around 8 K also exhibit ferromagnetic behavior at 300 K as shown in the Figure 4.11. In inset is given the variation of the volume susceptibility of the nanoparticles with temperature which gives a superconducting transition around 8 K.

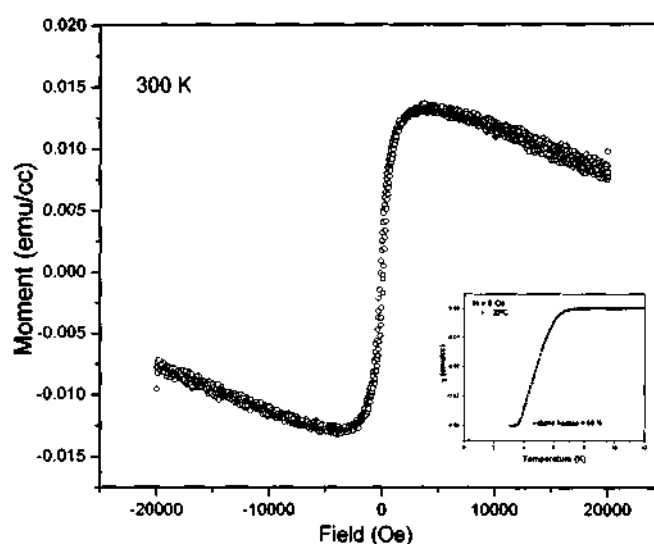


**Figure 4.11: Magnetization curve of NbN nanoparticles at 300 K with the inset showing the superconducting transition of the same at ~8 K**

The magnetic hysteresis found in nanoparticles of  $\text{MoN}_x$  and NbN are entirely the property of surface. We can therefore only say that the surface ferromagnetism occurs in superconducting nitrides, although below the superconducting transition temperature the magnetism could not be present. The presence of surface ferromagnetism as general



characteristics of nanoparticles of metal nitrides and oxides is a significant observation.

#### **4.6 Conclusions:**

The reaction between urea and  $\text{MoCl}_5$  is shown to readily give  $\gamma\text{-Mo}_2\text{N}$  under relatively mild conditions. In this reaction, urea decomposes to give  $\text{NH}_3$  at temperatures greater than 500 K along with the cyanic acid which decomposes further to give products like biuret [25]. The  $\text{NH}_3$  so produced reacts with  $\text{MoCl}_5$  to give  $\gamma\text{-Mo}_2\text{N}$ . The procedure has enabled the synthesis of nanoparticles of superconducting  $\gamma\text{-Mo}_2\text{N}$ . It is also noteworthy that the  $\gamma\text{-Mo}_2\text{N}$  nanoparticles readily transform to  $\delta\text{-MoN}$  nanoparticles on heating in  $\text{NH}_3$  at a relatively low temperature. The  $\delta\text{-MoN}$  so obtained seems to be somewhat disordered since the superconducting transition is around 5 K. It has also been found that the  $\text{MoN}_x$  nanoparticles show surface ferromagnetism.

## References

- [1]. L. E. Toth, *Transition Metal Carbides and Nitrides*, Academic Press, New York, 1971.
- [2]. S. T. Oyama, *The Chemistry of Transition Metal Carbides and Nitrides*, Blackie Academic Professional, Glasgow, 1996.
- [3]. H. O. Pierson, *Handbook of Refractory Carbides and Nitrides*, Noyes Publications, Westwood, 1996.
- [4]. K. S. Lee, H. Abe, J. A. Reimer, A. T. Bell, *J. Catal.* 139, 1993, 34.
- [5]. L. Volpe, M. Boudart, *J. Phys. Chem.* 90, 1986, 4874.
- [6]. S. T. Oyama, *Catal. Today*, 15, 1992, 179.
- [7]. M. Saito, R. B. Anderson, *J. Catal.* 63, 1980, 438.
- [8]. J. A. J. Rodriguez, G. M. Cruz, G. Bugli, M. Boudart, *Catal. Lett.* 45, 1997, 1.
- [9]. B. T. Matthias, J. K. Hulm, *Phys. Rev.* 87, 1952, 799.
- [10]. C. L. Bull, P. F. McMillan, E. Soignard, K. Leinenweber, *J. Solid State Chem.* 177, 2004, 1488.
- [11]. C. L. Bull, T. Kawashima, P. F. McMillan, D. Machon, O. Shebanova, D. Daisenberger, E. Soignard, E. T. Muromachi, L. C. Chapon, *J. Solid State Chem.* 179, 2006, 1762.
- [12]. D. A. Papaconstantopoulos, W. E. Pickett, B. M. Klein, L. L. Boyer, *Phys. Rev. (B)*. 31, 1985, 752.
- [13]. L. Volpe, M. Boudart, *J. Solid State Chem.* 59, 1985, 332.
- [14]. W. Lengauer, *J. Cryst. Growth*, 87, 1988, 295.

- [15]. R. Marchand, F. Tessier, F. J. DiSalvo, *J. Mater. Chem.*, 9, 1999, 297.
- [16]. N. S. Gajbhiye, R. S. Ningthoujam, *Phys. Stat. Sol.* 12, 2004, 3449.
- [17]. Ram Seshadri, *Curr. Opin. Solid State Mater. Sci.* 9, 2005, 1.
- [18]. M. Venkatesan, C. B. Fitzgerald, J. M. D. Coey, *Nature*, 430, 2004, 630.
- [19]. R. Monnier, B. Delley, *Phys. Rev. Lett.* 87, 2001, 157204.
- [20]. I. S. Elfimov, S. Yunoki, G. A. Sawatzky, *Phys. Rev. Lett.* 89, 2002, 216403.
- [21]. A. Zyweitz, J. Furthmuller, F. Bechstedt, *Phys. Rev. B* 62, 2000, 6854.
- [22]. J. M. D. Coey, M. Venkatesan, P. Stamenov, C. B. Fitzgerald, L. S. Dorneles, *Phys. Rev. B* 72, 2005, 024450.
- [23]. N. H. Hong, J. Sakai, N. Poirot, V. Breze, *Phys. Rev. B* 73, 2006, 132404.
- [24]. A. Sundaresan, R. Bhargavi, N. Rangarajan, U. Siddesh, C. N. R. Rao, *Phys. Rev. B* 74, 2006, 161306.
- [25]. S. Podsiadlo, *Thermochim. Acta*, 256, 1995, 367.

---

# **CHAPTER 5**

## **BN coating on one-dimensional nanostructures\***

---

### **Summary**

This chapter of the thesis deals with the coating of BN on one-dimensional nanostructures. A simple route involving urea as the nitrogen source has been employed to carry out boron nitride coating on carbon fibers, multi-walled carbon nanotubes and inorganic nanowires. The process involves heating the carbon fibers and nanotubes or inorganic nanowires in a mixture of  $\text{H}_3\text{BO}_3$  and urea, followed by a heat treatment at 1273 K in a  $\text{N}_2$  atmosphere. We have been able to characterize the BN coating by transmission electron microscopy as well as x-ray photoelectron spectroscopy. The urea decomposition route affords a simple method to coat boron nitride on one-dimensional nanostructures.

---

\* Paper based on this work has been submitted to Materials Science and Engineering A.

## **5.1 Introduction**

Discovery of carbon nanotubes [1] has attracted significant interest to nanoscale one-dimensional structures. Prospective miniaturization of electronic devices relies primarily on well-structured inorganic nanowires or nanotubes. Significant efforts have been made with respect to the synthesis of assembling multiple nanotubes and/or nanowires [2-5]. Boron nitride (BN) nanotubes in particular have received much attention because they are insulating, do not interact with molten metals and have higher oxidation resistance than carbon [6-7]. Such excellent properties promote the broad applications of BN, which include high-temperature insulators, self-lubricating and heat dissipating coatings, passivation layers, diffusion masks and wear-resistant coatings [8-9]. Thus BN coating should be valuable for using the nanowires as a separate layer between semiconductor nanowire and electronic substrate due to the insulating nature of the BN [10], and as a promoting component for large field-emitting enhancement factor due to its negative electron affinity [11].

## **5.2 Scope of the present study**

Hexagonal BN has a crystal structure similar to graphite; hence it is called 'white graphite'. However, it is an electrical insulator and intensively used as a carbon substitute for its much higher chemical inertness, especially at high temperature. BN is not wetted by many

metallic melts. Thus BN coating on nanowires or nanotubes would be of much use. There has been some effort in the literature in this direction. Chen et al. [12] have coated BN on carbon nanotubes (CNTs) by means of boric acid ( $\text{H}_3\text{BO}_3$ ) infiltration followed by treatment with  $\text{NH}_3$  at 1200 °C while Yoo et al. [13] coated BN films on CNTs using a radio frequency sputtering. BN-coated SiC nanowires have been prepared by heating a mixture of Si and  $\text{In}_2\text{O}_3$  powders in a BN crucible [14]. Gao et al. obtained the BN/ $\text{Si}_3\text{N}_4$  nanocomposite by nitriding a  $\text{Si}_3\text{N}_4/\text{NH}_4\text{HB}_4\text{O}_7$  mixture in ammonia gas [15].  $\text{Al}_2\text{O}_3/\text{BN}$  nanocomposites have been fabricated by hot-pressing  $\alpha\text{-Al}_2\text{O}_3$  powders covered partly with turbostratic BN (t-BN) [16]. GaN-BN core-shell nanocables were synthesized by thermal chemical vapor deposition using GaN/ $\text{B}_2\text{O}_3/\text{NH}_3$  reaction [17]. Zhang et al. have reported the synthesis of semiconductor GaN nanowires sheathed with BN layers by chemical vapor deposition [18].

We felt that it would be worthwhile to develop a simple method to coat carbon fibers and inorganic nanowires with BN. For this purpose, we have used the urea route, wherein we coat the nanostructures with a mixture of  $\text{H}_3\text{BO}_3$  and urea followed by heating in a  $\text{N}_2$  atmosphere. By this means, the ammonia generated in-situ reacts with the  $\text{B}_2\text{O}_3$  produced concomitantly, giving rise to the BN coating. In this chapter, we report the results of our investigations on the coating of carbon fibers,

multi-walled carbon nanotubes and nanowires of silicon carbide, silicon nitride, aluminium oxide and gallium nitride by the urea route.

### **5.3 Experimental and related aspects**

#### **(a) Coating BN on one-dimensional nanostructures:**

Multi-walled carbon nanotubes (MWNTs) were prepared by the arc-discharge method and functionalized by nitric acid treatment as reported in the literature [19]. MWNTs so obtained had an outer diameter of 25 nm. Carbon fibers prepared by the pyrolysis of PANI were obtained from National Physical Laboratory, New Delhi. The fibers had a diameter of 7  $\mu\text{m}$ .  $\text{Al}_2\text{O}_3$ , SiC and GaN nanowires were synthesized by the carbothermal reduction method [20-22]. Treating the nanowires and carbon fibers with dilute  $\text{HNO}_3$  functionalized their surfaces. The acid-treated MWNTs and inorganic nanowires were dried under dynamic vacuum at 353 K. The basic procedure employed for producing BN coating was to treat the carbon fibers or the inorganic nanowires with a mixture of  $\text{H}_3\text{BO}_3$  and urea in the molar ratio of 1:6, followed by heat treatment at 1273 K for 3 h in a  $\text{N}_2$  atmosphere. The 1:6  $\text{H}_3\text{BO}_3$ -urea mixture was prepared by concentrating an aqueous solution containing 100 mg of  $\text{H}_3\text{BO}_3$  and 600 mg of urea by heating. The acid-treated carbon fibers were kept in the  $\text{H}_3\text{BO}_3$ -urea mixture for an appropriate time period depending on the desired coating thickness. In order to get a

heavy coating, the fibers were kept in the mixture for about 3 h at 343 K. In order to reduce the thickness of the coating, the fibers were taken out after dipping them in the H<sub>3</sub>BO<sub>3</sub>-urea mixture for 1h. The carbon fibers so treated were placed in an alumina boat and heated in a tube furnace at 1273 K for 3h under flowing N<sub>2</sub>. For coating MWNTs and nanowires with BN, the acid-treated nanotubes and nanowires were treated with the H<sub>3</sub>BO<sub>3</sub>-urea mixture for 1h, followed by heat treatment at 1273 K for 3 h in a N<sub>2</sub> atmosphere.

#### **(b) Characterization Techniques:**

**X-ray Diffraction:** X-ray diffraction (XRD) patterns of the nitrides were recorded using Cu K $\alpha$  radiation on a Rich-Siefert XRD-3000-TT diffractometer.

**Scanning electron microscopy:** Scanning electron microscope (SEM) images were obtained using a LEICA S440i SEM.

**Transmission electron microscopy:** For transmission electron microscopy, the nitrides were dispersed in CCl<sub>4</sub> and dropped on to the holey carbon-coated copper grids. The grids were allowed to dry in the air. Transmission electron microscope (TEM) images were obtained with a JEOL JEM 3010, operating with an accelerating voltage of 300 kV.

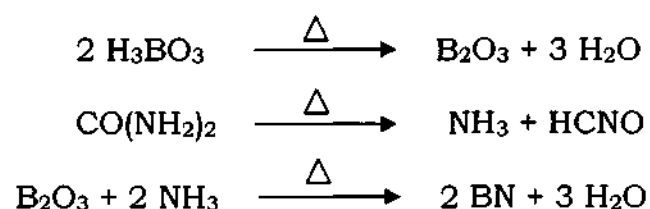


**X-ray photoelectron spectroscopy:** X-ray photoelectron spectra (XPS) were recorded with an ESCALAB MKIV spectrometer employing Al K $\alpha$  radiation (1486.6 eV).

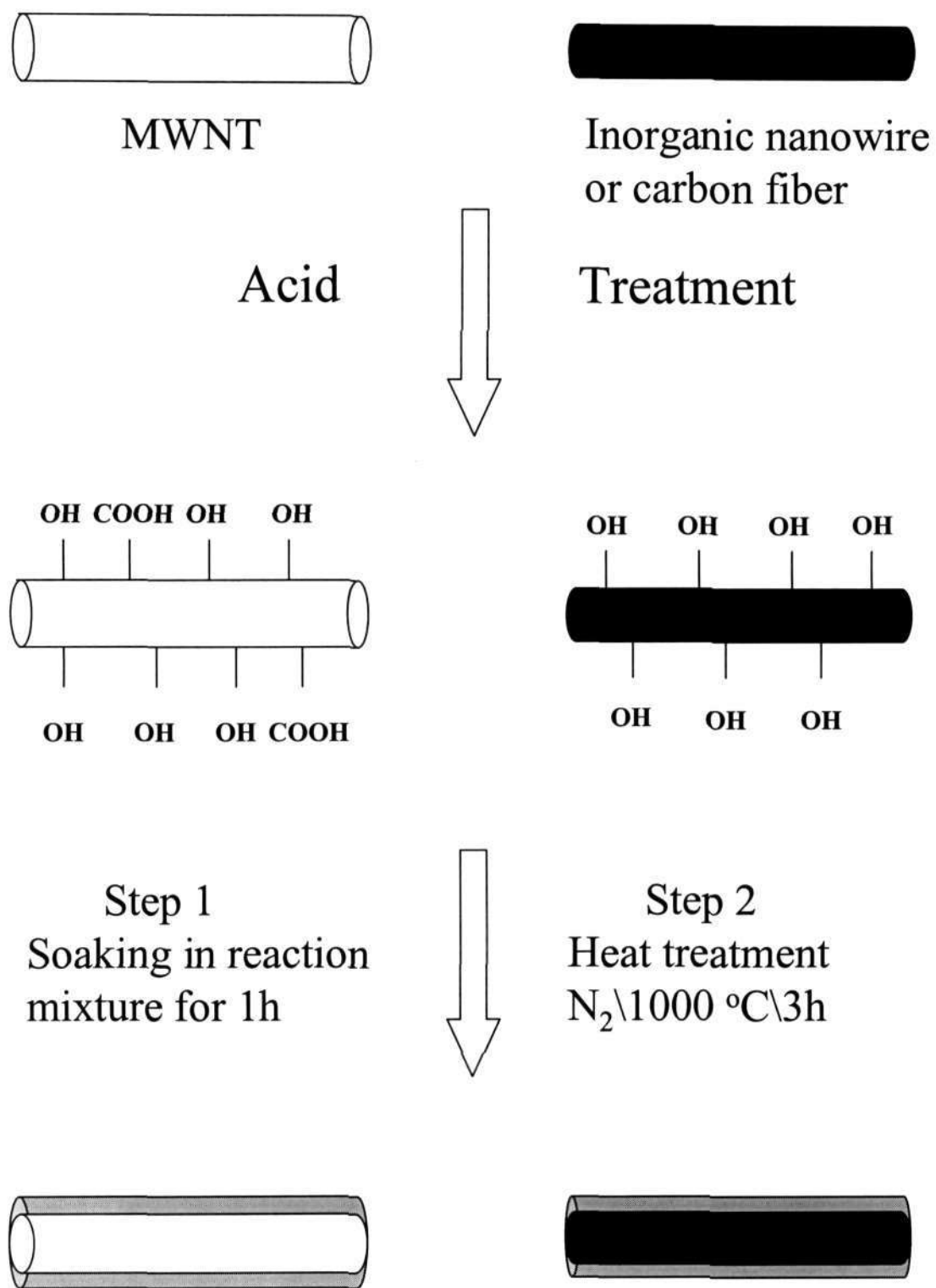
## **5.4 Results and Discussions**

### **(a) Characterization of the BN carbon fibers:**

Carbon fibers and MWNTs on acid treatment get functionalized with surface hydroxyl and carboxyl groups while the metal oxide nanowires necessarily possess hydroxyl groups on their surfaces [23-25]. We have made use of the surface functional groups on the carbon fibers, MWNTs and inorganic nanowires for reaction with the 1:6 H<sub>3</sub>BO<sub>3</sub>-urea mixture. On heating, H<sub>3</sub>BO<sub>3</sub> gives B<sub>2</sub>O<sub>3</sub> which reacts with NH<sub>3</sub> produced by the decomposition of urea to give BN as shown below:

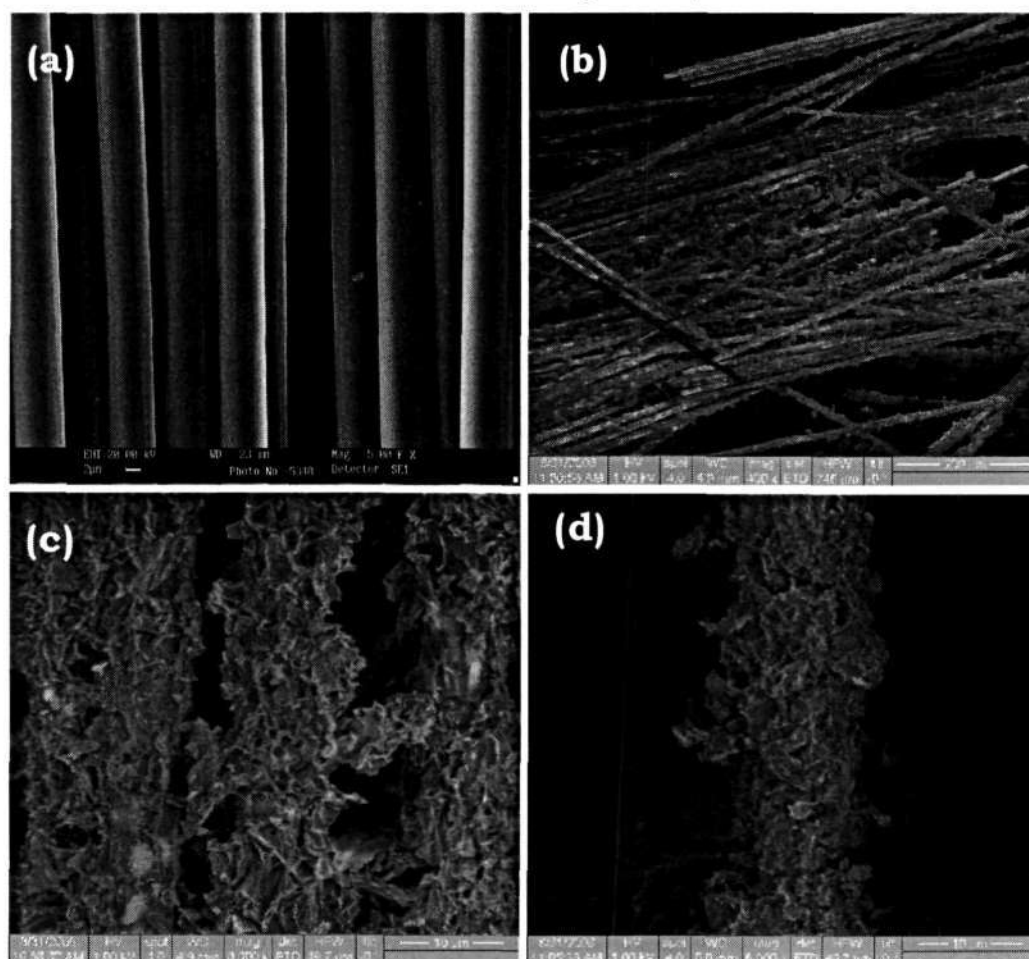


This process is depicted schematically in Figure 5.1.



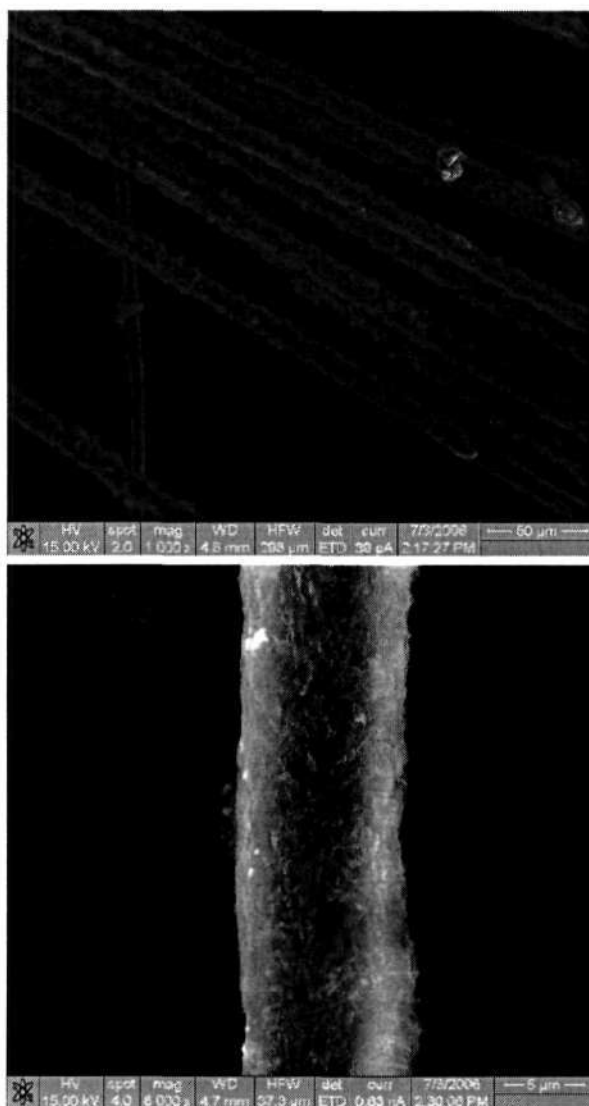
**Figure 5.1: Schematic representation of the entire coating process.**

In Figure 5.2 (a) is shown the acid treated carbon fibers and average outer diameter is  $\sim 7\mu\text{m}$ . Figures 5.2 (b) and (c) show the FESEM images of heavily coated carbon fibers. The heavy coating was obtained by the reaction of the carbon fibers with the 1:6  $\text{H}_3\text{BO}_3$ -urea mixture for 3 h followed by the heat treatment at 1273 K for 3 h in flowing  $\text{N}_2$ . In Figure 5.2 (d) is given the FESEM image of a single strand of a heavily coated carbon fiber. The thickness of the coating is  $\sim 2\mu\text{m}$ .



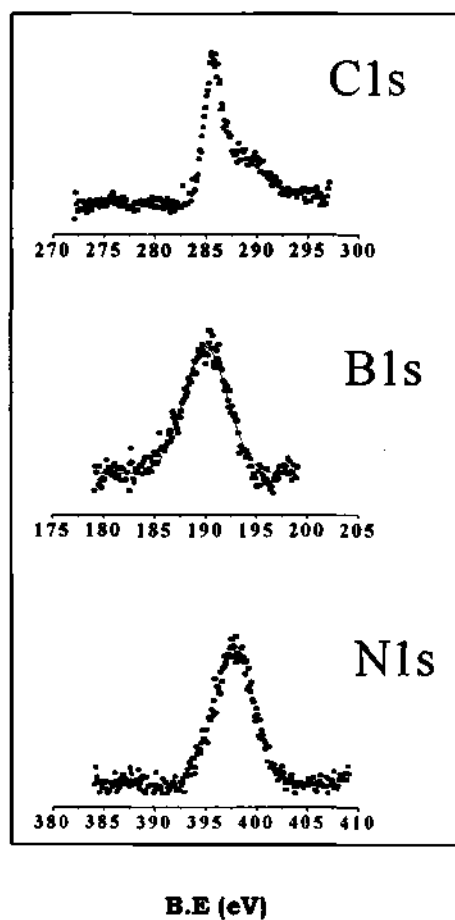
**Figure 5.2: SEM images of (a) acid-treated carbon fibers (b) and (c) heavily coated carbon fibers (d) heavily coated single strand of the fiber.**

Figure 5.3 (a) gives the FESEM image of the carbon fibers with thinner coating obtained by the reaction of the acid-treated carbon fibers with the 1:6  $H_3BO_3$ -urea mixture for 1h and then heated at 1273 K for 3 h in an inert atmosphere. In Figure 5.3 (b) we show a FESEM image of a carbon fiber with thinner coating. The thickness of the coating here is around 1  $\mu m$ .



**Figure 5.3: SEM images of (a) carbon fibers with thinner coating (b) single strand of less coating.**

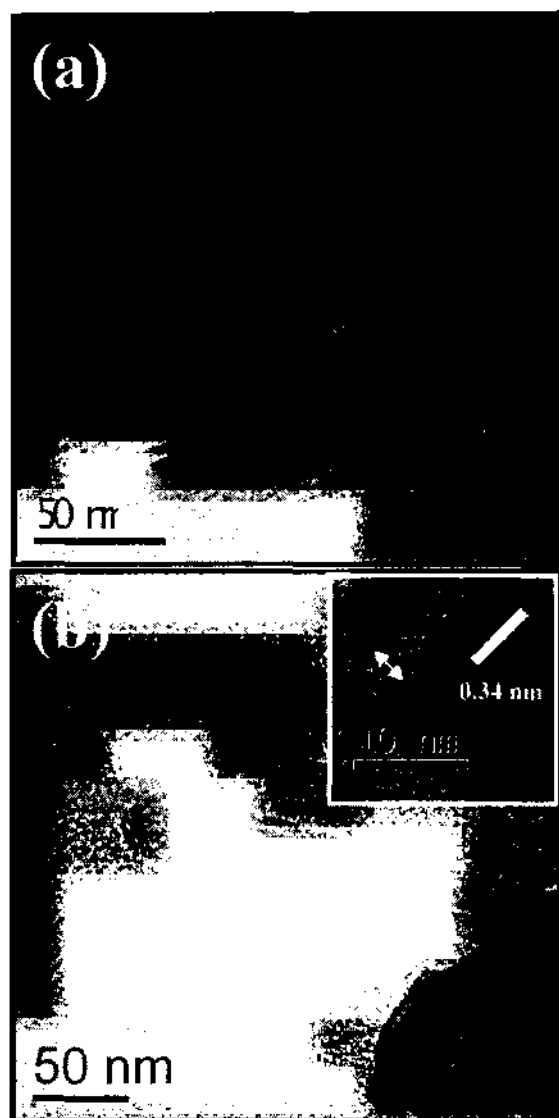
We have characterized the BN-coated carbon fibers by XPS. Figure 5.4 gives the XP spectrum of the-BN coated carbon fibers. The spectrum shows characteristic binding energies (BE) of 285 eV for C (1s), 190.3 eV for B (1s) and 397.4 eV for N (1s) corresponding to BN.



**Figure 5.4: XP spectrum of the heavily coated carbon fibers.**

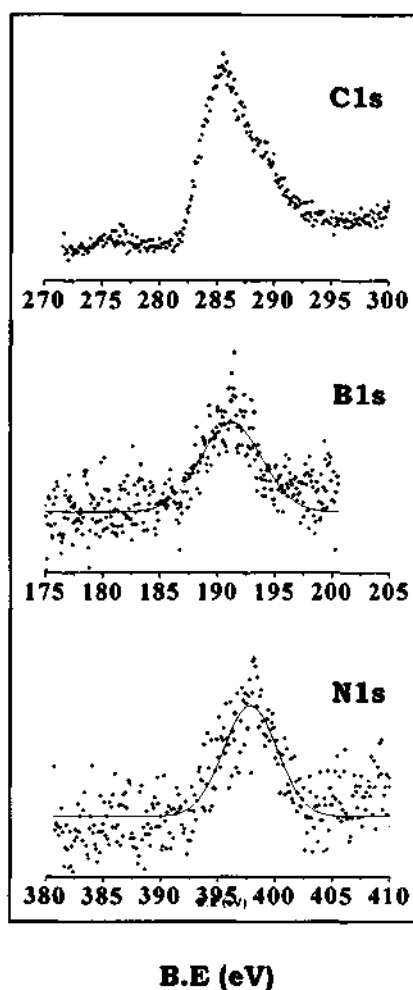
Treatment of acid-treated MWNTs with the 1:6  $H_3BO_3$ -urea mixture for 1h followed by heating at 1273 K for 3 h in a  $N_2$  atmosphere gave BN-coated MWNTs. In Figure 5.5 (a) and (b) are shown the TEM images of the BN-coated MWNTs. The thickness of the BN coating is around 10

nm. The inset in Figure 5.5 (b) is the high resolution electron microscope (HREM) image of a BN-coated MWNT. The lattice spacing of the graphitic layers of the MWNT is 0.34 nm corresponding to the (002) planes.



**Figure 5.5: (a) and (b) are the TEM images of the BN coated MWNTs with the inset in b) showing the HREM image of a BN coated MWNT.**

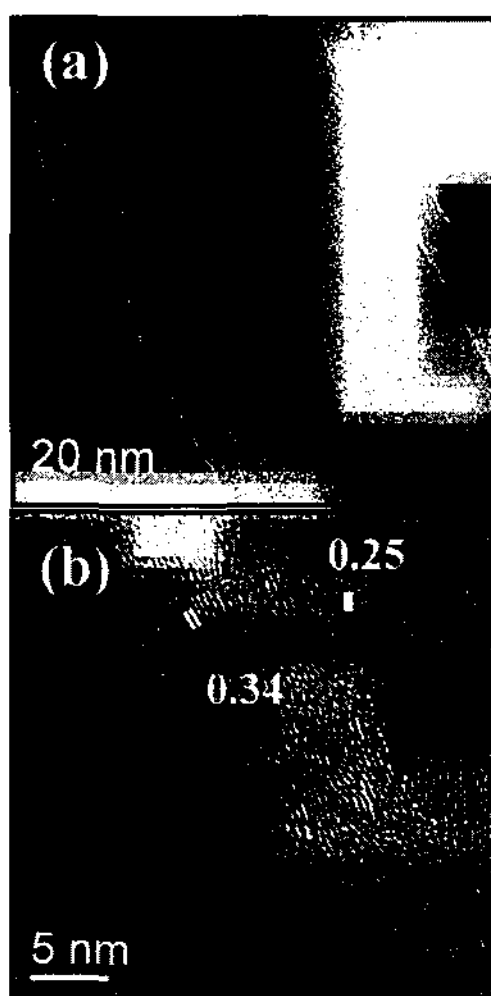
In Figure 5.6 we have given the XP spectrum of the BN-coated MWNTs which gives characteristic BE of 285 eV for C (1s), 190 eV for B (1s) and 397.8 eV for N (1s) corresponding to BN.



**Figure 5.6: XP spectrum of the BN-coated MWNTs.**

Acid-treated inorganic nanowires were also reacted with the 1:6  $\text{H}_3\text{BO}_3$ -urea mixture for 1h followed by a heat treatment at 1273 K for 3 h in a  $\text{N}_2$  atmosphere. In Figure 5.7 (a) we give the TEM image of a BN-

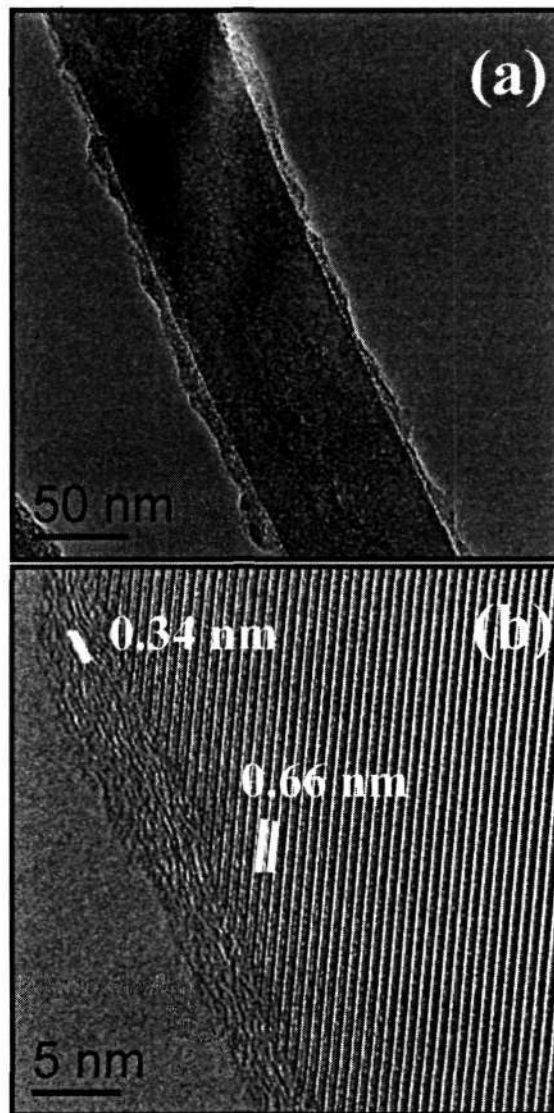
coated SiC nanowire. The coating thickness is ~10 nm. Figure 5.7 (b) is the HREM image of the BN-coated SiC nanowire. It shows a lattice spacing of 0.25 nm corresponding to the (111) planes of the SiC and a spacing of 0.34 nm corresponding to the (002) planes of the BN. The lattice image suggests BN to be turbostratic. The XP spectrum of the BN coated SiC nanowire gave the characteristic BE of 190 eV for B (1s) and 397.6 for N (1s) corresponding to BN.



**Figure 5.7: (a) TEM image of a BN coated SiC nanowire. (b) HREM image of the BN-coated SiC nanowire.**

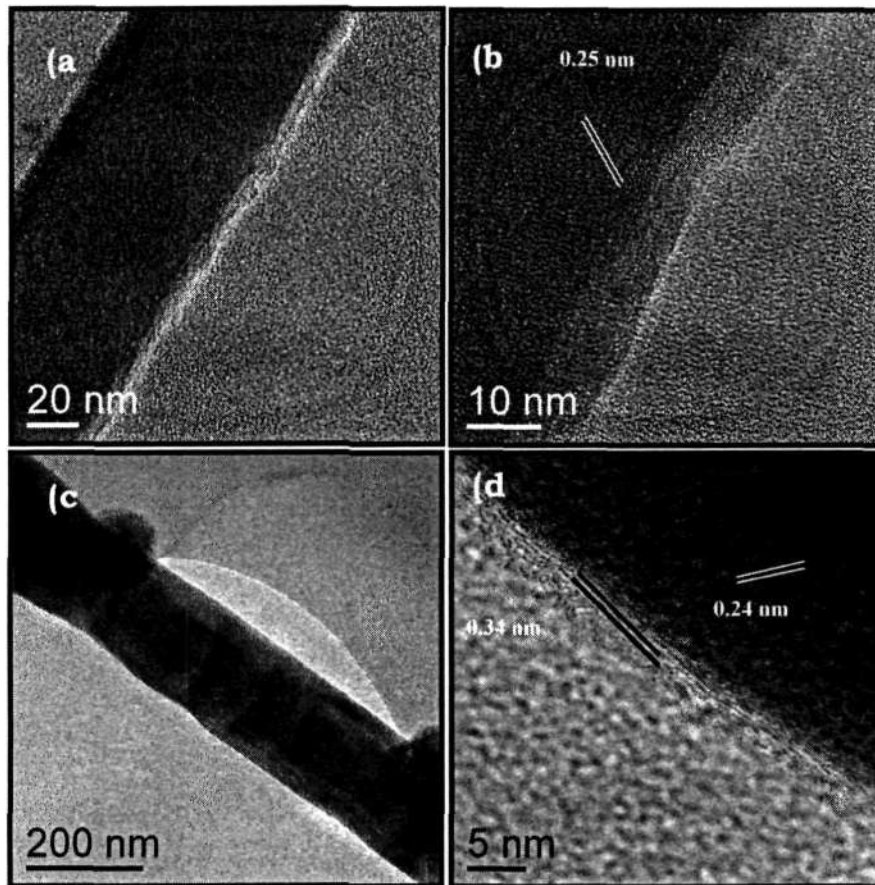


Figure 5.8 (a) gives a TEM image of a BN-coated  $\text{Si}_3\text{N}_4$  nanowire. From the TEM image it is seen that the coating thickness is  $\sim 8$  nm. The HREM image of the BN-coated  $\text{Si}_3\text{N}_4$  nanowire in Figure 5.8 (b) shows a spacing of 0.66 nm corresponding to the (100) planes of  $\text{Si}_3\text{N}_4$  and a spacing of 0.34 nm corresponding to the (002) planes of the BN.



**Figure 5.8: (a) TEM image of a BN coated  $\text{Si}_3\text{N}_4$  nanowire. (b) HREM image of the BN-coated  $\text{Si}_3\text{N}_4$  nanowire.**

In Figure 5.9 (a) we show the TEM image of a BN-coated  $\text{Al}_2\text{O}_3$  nanowire. The BN coating seems to be amorphous since the HREM image shown in Figure 5.9 (b) shows only lattice spacing of 0.25 nm corresponding to the (104) planes of  $\text{Al}_2\text{O}_3$ . The TEM image of a BN-coated GaN nanowire in Figure 5.9 (c) indicates the coating thickness to be 3 nm. The HREM image shown as an inset of Figure 5.9 (d) gives a lattice spacing of 0.24 nm corresponding to the (110) planes of GaN and a spacing of 0.34 nm corresponding to the (002) planes of the BN.



**Figure 5.9: (a) TEM image of a BN coated  $\text{Al}_2\text{O}_3$  nanowire (b) HREM image of the BN-coated  $\text{Al}_2\text{O}_3$  nanowire (c) TEM image of a BN coated GaN nanowire (d) HREM image of the BN-coated GaN nanowire.**

## **5.5 Conclusions**

In conclusion, we have been able to develop a simple route involving the reaction of  $\text{H}_3\text{BO}_3$  with urea to coat carbon nanotubes as well as nanowires of  $\text{SiC}$ ,  $\text{Si}_3\text{N}_4$ ,  $\text{Al}_2\text{O}_3$  and  $\text{GaN}$  with  $\text{BN}$ , the coating thickness being generally few nanometers. We have been able to get the high resolution electron microscope images of the  $\text{BN}$  coating in most of the cases. Carbon fibers could also be coated with  $\text{BN}$  with a coating thickness of few microns by the urea route.

## References

- [1]. S. Iijima, *Nature*, 354, 1991, 56.
- [2]. Z. Yao, H. W. Ch. Postma, L. Balents, C. Dekker, *Nature*, 402, 1999, 273.
- [3]. M. S. Gudiksen, L. J. Lauhon, J. Wang, D. C. Smith, C. M. Lieber, *Nature*, 415, 2002, 617.
- [4]. J. T. Hu, M. Ouyang, P. D. Yang, C. M. Lieber, *Nature*, 399, 1999, 48.
- [5]. L. J. Lauhon, M. S. Gudiksen, D. Wang, C. M. Lieber, *Nature*, 420, 1999, 57.
- [6]. L. A. Chernozatonskii, E. G. Galpern, I. V. Stankevich, Y. K. Shimkus, *Carbon*, 37, 1999, 117.
- [7]. D. Goldberg, Y. Bando, M. Mitome, K. Kurashima, N. Grobert, M. Reyes-Reyes, H. Terrones, M. Terrones, *Chem. Phys. Lett.*, 360, 2002, 1.
- [8]. S. P. S. Arya, A. D. Amico, *Thin Solid Films*, 157, 1988, 267.
- [9]. P. B. Mirkarimi, K. F. McCarty, D. L. Medlin, *Mater. Sci. Eng.*, 21, 1997, 47.
- [10]. X. Blase, A. Rubio, S. G. Louie, M. L. Cohen, *Europhys. Lett.* 28, 1998, 335.
- [11]. M. J. Powers, M. C. Benjamin, L. M. Porter, R. J. Nemanich, R. F. Davis, J. J. Cuomo, G. L. Doll, S. J. Harris, *Appl. Phys. Lett.* 67, 1995, 3912.

- [12]. L. Chen, H. Ye, Y. Gagotsi, *J. Am. Ceram. Soc.*, 87, 2004, 147.
- [13]. J. B. Yoo, J. H. Han, S. H. Choi, T. Y. Lee, C. Y. Park, T. W. Jeong, J. H. Lee, S. Yu, G. Park, W. K. Yi, H. S. Kim, Y.-J. Baik, J. M. Kim, *Physica B*, 323, 2002, 180.
- [14]. Y. Li, P. S. Dorozhkin, Y. Bando, D. Golberg, *Adv. Mater.* 17, 2005, 545.
- [15]. L. Gao, X. Jin, J. Li, Y. Li, J. Sun, *Materials Science and Engineering A* 415, 2006, 145.
- [16]. T. Kusunose, Y-H. Kim, T. Sekino, T. Matsumoto, N. Tanaka, T. Nakayama, K. Niihara, *J. Mater. Res.*, 20, 2005, 183.
- [17]. W. S. Jang, Y. S. Kim, J. Lee, J. Park, C. J. Lee, C. J. Park, *Chem Phys Lett.* 422, 2006, 41.
- [18]. J. Zhang, L. Zhang, F. Jiang, Z. Dai, *Chem. Phys. Lett.* 383, 2004, 423.
- [19]. B. C. Satishkumar, A. Govindaraj, E. M. Vogl, L. Basumallick, C. N. R. Rao, *J. Mater. Res.* 12, 1997, 604.
- [20]. G. Gundiah, F. L. Deepak, A. Govindaraj, C. N. R. Rao, *Top. Catal.* 24, 2003, 137.
- [21]. F.L. Deepak, A. Govindaraj, C.N.R. Rao, *J. Nanosci. Nanotech.* 1, 2001, 303.
- [22]. G. Gundiah, G.V. Madhav, A. Govindaraj, Md. Motin Sheikh, C.N.R. Rao, *J. Mater. Chem.* 12, 2002, 1606.

- [23]. R. C. Haddon (Ed.), Special issue on "Carbon Nanotubes", *Acc. Chem. Res.* 35, 2002, 997.
- [24]. C. N. R. Rao, B. C. Satishkumar, A. Govindaraj, M. Nath, *ChemPhysChem.* 2, 2001, 78.
- [25]. *Nanowires and Nanobelts — Materials, Properties and Devices* (Ed: Z. L. Wang), Kluwer Academic, Boston, MA, 2003.

620.11  
p06

JNCASR  
Acc  
No 4344  
LIBRARY

92  
7  
101